INTERNATIONAL ATOMIC ENERGY AGENCY
UNITED NATIONS EDUCATIONAL, SCIENTIFIC AND CULTURAL ORGANIZATION

INTERNATIONAL CENTRE FOR THEORETICAL PHYSICS
34100 TRIESTE (ITALY) - P.O.B. 586 - MIRAMARE - STRADA COSTIERA 11 - TELEPHONE: 2240-1
CABLE: CENTRATOM - TELEX 460392-1

SMR/206-17

"SCHOOL ON POLYMER PHYSICS"

27 April - 15 May 1987

"A COMPREHENSIVE EXPERIMENTAL STUDY OF THE RHEOLOGICAL BEHAVIOUR OF HDPE"

I. Entrance Effect and Shear Viscosity Results

Professor D. ACIERNO
Istituto di Ingegneria Chimica
Università di Palermo
Palermo, Italy

Rheologica Acta

Rheol. Acta 22, 299 – 307 (1983)

A comprehensive experimental study of the rheological behaviour of HDPE. I. Entrance effect and shear viscosity results

F. P. La Mantia, A. Valenza, and D. Acierno

Istituto di Ingegneria Chimica, Università di Palermo (Italy)

Abstract: Rheological properties of six high-density-polyethylene (HDPE) samples with known average molecular weight and molecular weight distribution have been determined with the aid of two capillary viscometers over a wide range of temperatures and shear rates. Generalized relationships have been found for the entrance correction, the zero-shear viscosity and the shift factors of the whole viscosity curve.

Key words: High-density-polyethylene, end effect, shear viscosity

1. Introduction

It is well known that the rheological behaviour of a molten polymer depends strongly on structural parameters such as average molecular weight, molecular weight distribution, degree of branching, etc. [1–4]. However, the dependence of shear viscosity, die swell, elongational viscosity, etc. on the above parameters is in most cases not even qualitatively very well established [3, 5].

We have undertaken a comprehensive research program on the rheological behaviour of high-density-polyethylene (HDPE). In this paper, we attempt to assess, both qualitatively and quantitatively, the entrance effects and the shear-viscosity dependence on molecular weight and molecular weight distribution. The effect of temperature is also taken into account throughout.

2. Experimental

The materials used in this work were six high density polyethylene samples differing in average molecular weight and/or molecular weight distribution. These characteristics, listed in table 1, had been evaluated [6] with the usual chromatographic procedures.

A constant force viscometer and a constant rate viscometer have been employed for determining the rheological characteristics of the above polymers: more precisely, the former has been used in the low shear rate region and the latter in the high shear rate region. Four different capillaries have been adopted in both cases: the diameter was always 1 mm and the length to diameter ratios were 40, 20, 10 and 5; the entrance angle was 180°. The test temperatures were 160, 170, 180 and 190 °C.

Table 1

Sample code	M_w	$\beta = M_w/M_n$
A	65,000	4.3
B	113,000	5.3
C	147,000	4.7
D	158,000	7.9
E	195,000	15.6
F	395,000	22.7

3. Results and discussion

Typical results are reported in the form of pressure drop vs. flow rate for all the capillaries in figure 1 and in the form of pressure drop vs. length-to-diameter ratio at given flow rates in figure 2.

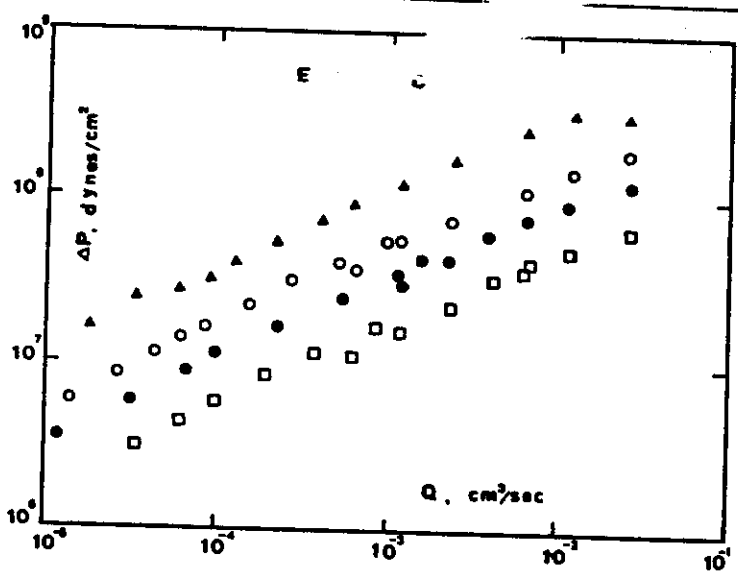

Fig. 1. Pressure drop vs. flow rate for 4 capillaries. Curves from top to bottom correspond to L/D = 40, 20, 10 and 5

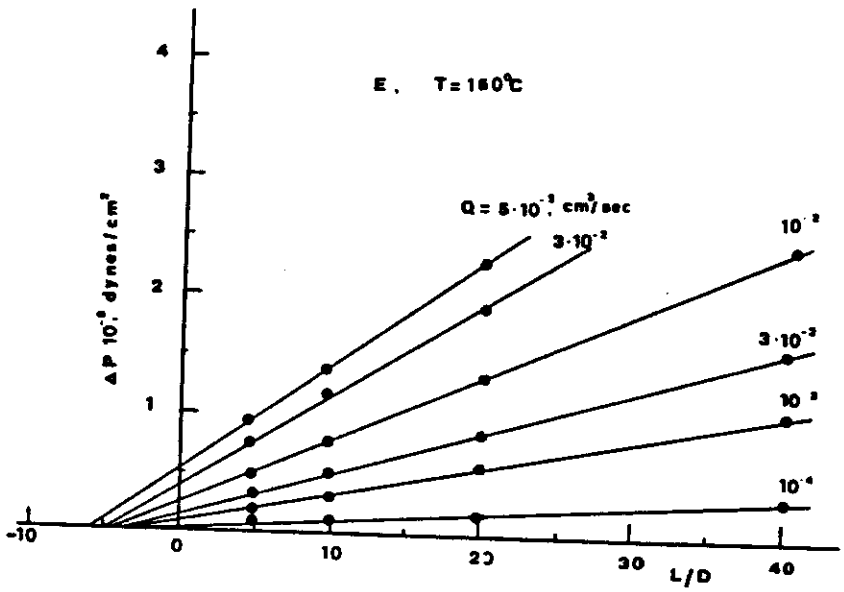

Fig. 2. Pressure drop vs. length to-diameter ratio for various flow rates

Following the Bagley analysis [7], the latter type of diagram enables one to evaluate the end correction factor n, see eq. (9) below.

The factor n is shown in figure 3 for all the polymers and test temperatures as a function of the apparent shear rate, $\dot{\gamma}_{app}$, which is easily calculated from the flow rate [8].

As one might expect, n decreases with increasing temperature. More quantitatively, a generalized dependence on the temperature has been found through the use of a single shift factor for all samples, defined as [9]

$$\log a_T = -\frac{C_1(T - T_r)}{C_2 + (T - T_r)}. \quad (1)$$

The constants C_1 and C_2 take the values 2.4 and -103, respectively, for a reference temperature T_r = 190 °C.

The generalized curves, n vs. $\dot{\gamma}_{app}a_T$, are shown in figure 4. From the data of figure 4 it appears that the Bagley factor increases with both the weight-average molecular weight and the molecular weight distribution parameter, $\beta = M_w/M_n$. A quantitative form for this dependence has been found by constructing semi-

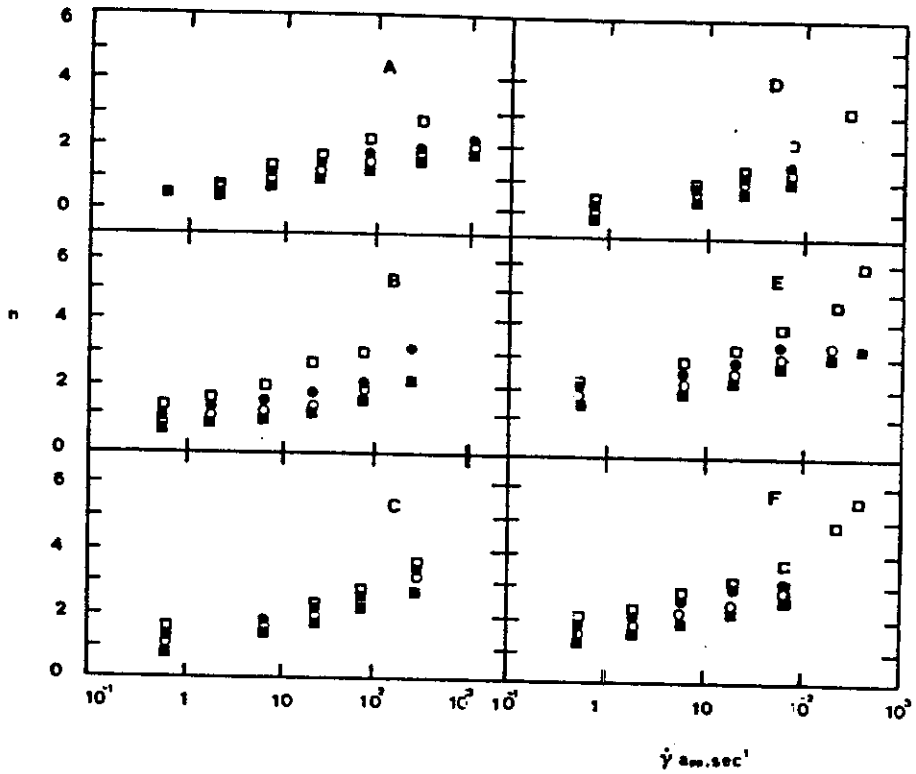

Fig. 3. End correction factor as a function of the apparent shear rate at various temperatures, □ 160°C, ● 170°C, ○ 180°C, ■ 190°C

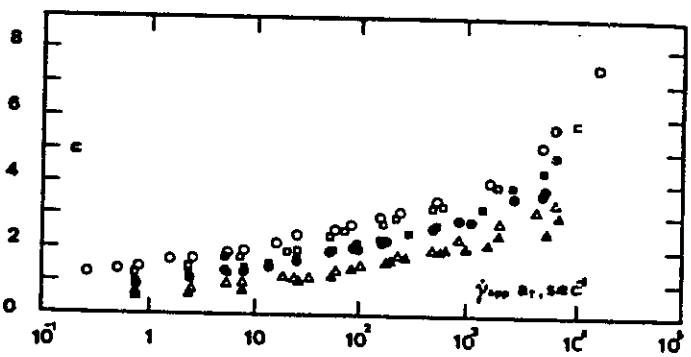

Fig. 4. Generalized curves for the end correction factor. ▲ sample A, △ sample B, ● sample C, ■ sample D, □ sample E, ○ sample F

logarithmic plots of n vs. $M_w\beta$ at fixed values of $\dot{\gamma}_{app}a_T$.

Since the best fitting curves through the experimental points are straight lines (see figure 5), one may write

$$n = K_n + C_n \ln(M_w\beta)\,. \qquad (2)$$

The constants K_n and C_n depend upon temperature and shear rate through the product $\dot{\gamma}_{app}a_T$ in the following form:

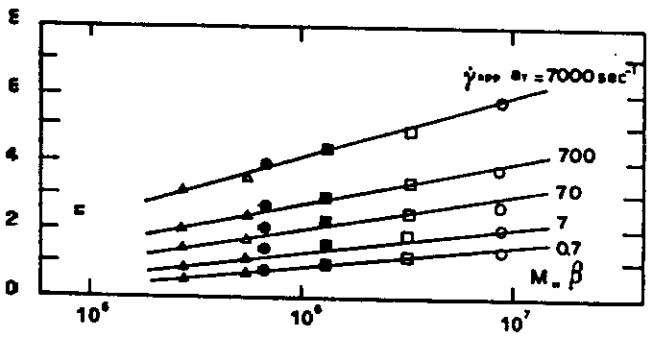

Fig. 5. End correction factor as a function of $M_w\beta$ at various shear rates. Key for symbols as in figure 4

$$K_n = -2.76 - 0.435 \ln(\dot{\gamma}_{app} a_T), \quad (3)$$

$$C_n = 0.271 (\dot{\gamma}_{app} a_T)^{0.12}. \quad (4)$$

In conclusion, it is possible, with the aid of eqs. (1–4), to evaluate the end correction factor for any HDPE and for any working condition, i.e. any tem-

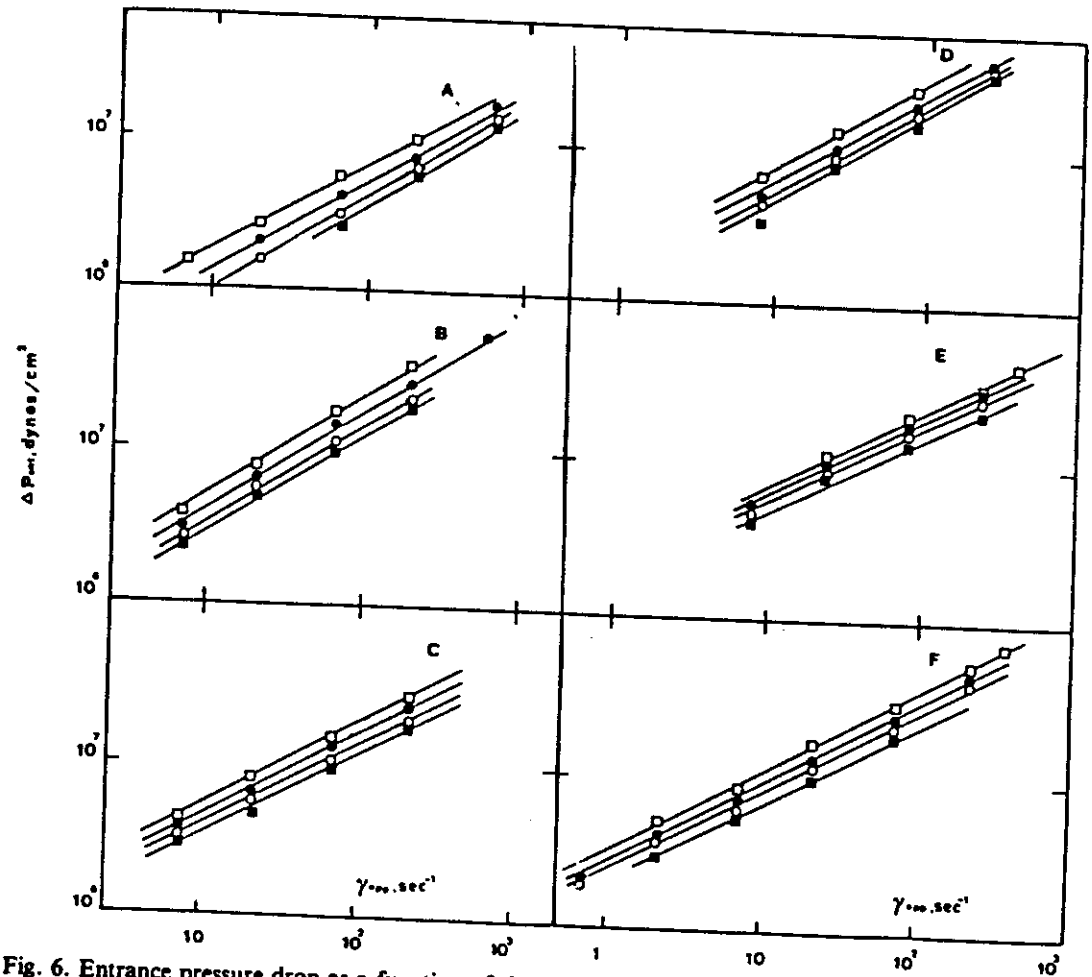

Fig. 6. Entrance pressure drop as a function of the shear rate

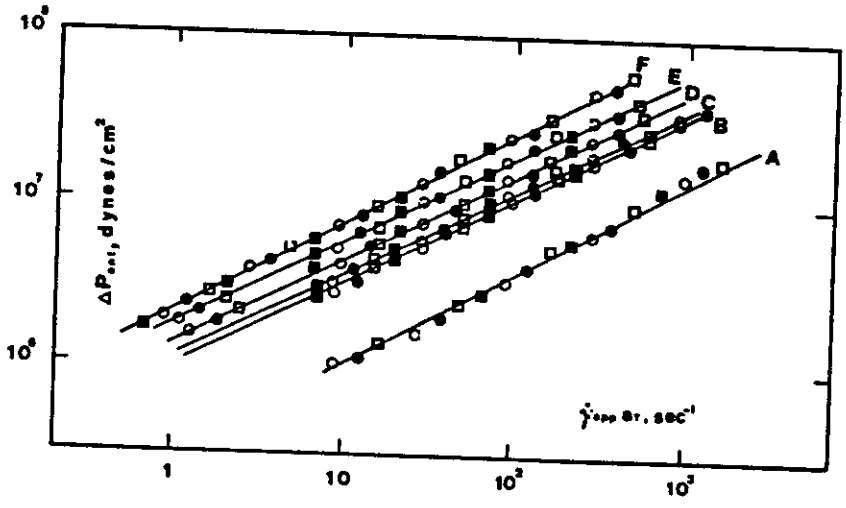

Fig. 7. Generalized curves for entrance pressure drop. Key for symbols as in figure 3

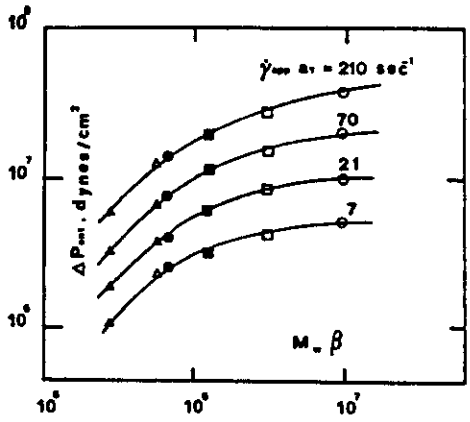

Fig. 8. Entrance pressure drop as a function of $M_w\beta$ at various shear rates. Key for symbols as in figure 4

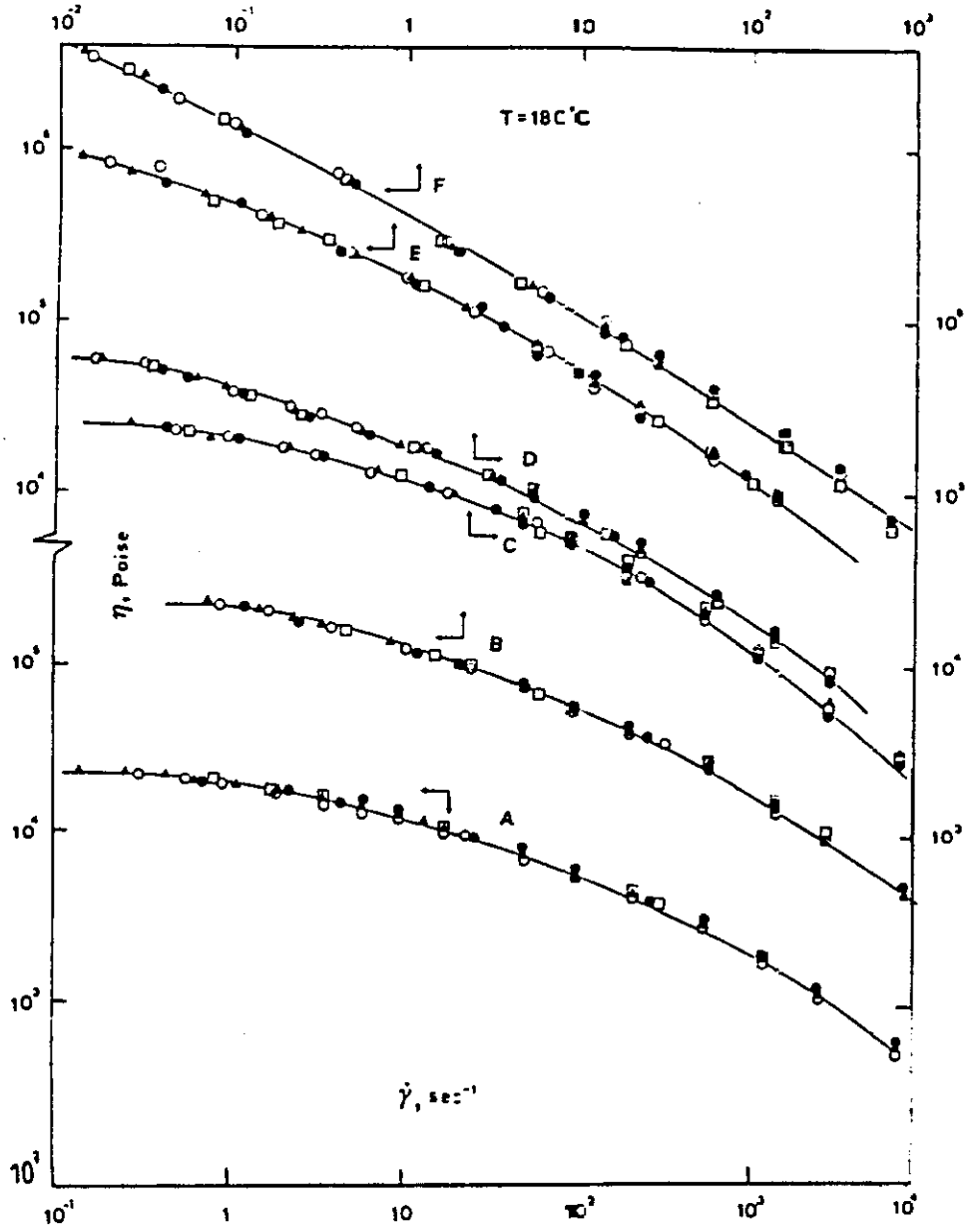

Fig. 9. Viscosity vs. shear rate. Key for symbols as in figure 1

perature and apparent shear rate. It has to be said, however, that should M_w become very small, n must approach zero. Thus eq. (2) cannot hold in that limit.

A different way of considering entry effects, which can also be used to estimate normal stresses [10, 11], is that of determining the pressure drop at the capillary entrance. This is obtained from the plots in figure 2 by taking the value of Δp at $L/D = 0$ [3]. Though this value is the sum of the entrance and the exit pressure drops [3], since the ratio $\Delta p_{exit}/\Delta p_{ent}$ is very small, one may approximately assume $\Delta p_{L/D=0} = \Delta p_{ent}$.

The values of Δp_{ent} for all test temperatures and polymeric samples are reported in figure 6 as function of the apparent shear rate. For each temperature and polymeric sample one may write the relationship:

$$\Delta p_{ent} = K(\dot{\gamma}_{app})^c , \tag{5}$$

where K depends both on the temperature and the polymer while c is 0.53 in all cases, in good agreement with similar published results [12].

As in the case of the Bagley factor, curves for different temperatures may be collapsed into a single one. The generalized curves, obtained by using the same shift factor for all materials, are shown in figure 7: the reference temperature is 190 °C. Also this shift factor, a_T^i, follows eq. (1) with $C_1 = 3.12$ and $C_2 = -230$.

Once again the entrance pressure drop can be shown to depend on structural parameters through the $M_w\beta$ product (see figure 8):

$$\Delta p_{ent} = K_{ent} + C_{ent} \ln(M_w\beta) \tag{6}$$

and, also in this case, K_{ent} and C_{ent} depend only on the factor $\dot{\gamma}_{app}a_T^i$:

$$K_{ent} = -5.3\,(\dot{\gamma}_{app}a_T^i)^{0.53} , \tag{7}$$

$$C_{ent} = 0.488\,(\dot{\gamma}_{app}a_T^i)^{0.53} . \tag{8}$$

By the use of either the Bagley factor, n, or the Δp_{ent} one can calculate the shear stress at the wall as

$$\tau = \frac{D\Delta p}{4(L + nD)} = \frac{D(\Delta p - \Delta p_{ent})}{4L} . \tag{9}$$

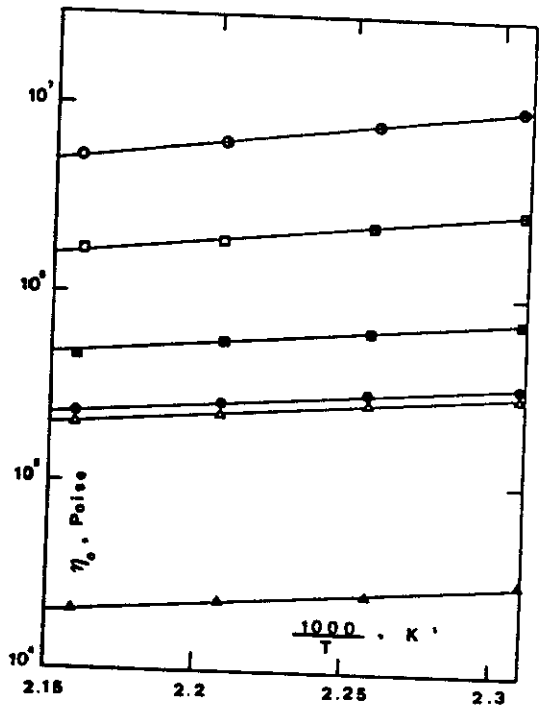

Fig. 10. Zero-shear viscosity as a function of the inverse of absolute temperature. Key for symbols as in figure 4. Semi-closed symbols correspond to data evaluated through eq. (11)

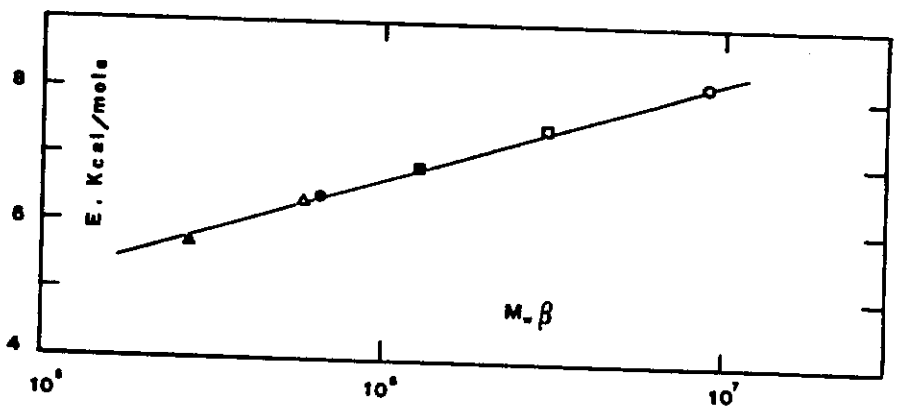

Fig. 11. Activation energy vs. $M_w\beta$. Key for symbols as in figure 4

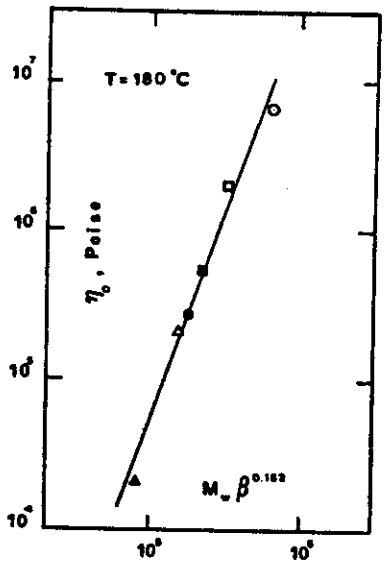

Fig. 12. Zero-shear viscosity vs. $M_w\beta^{0.152}$. Key for symbols as in figure 4

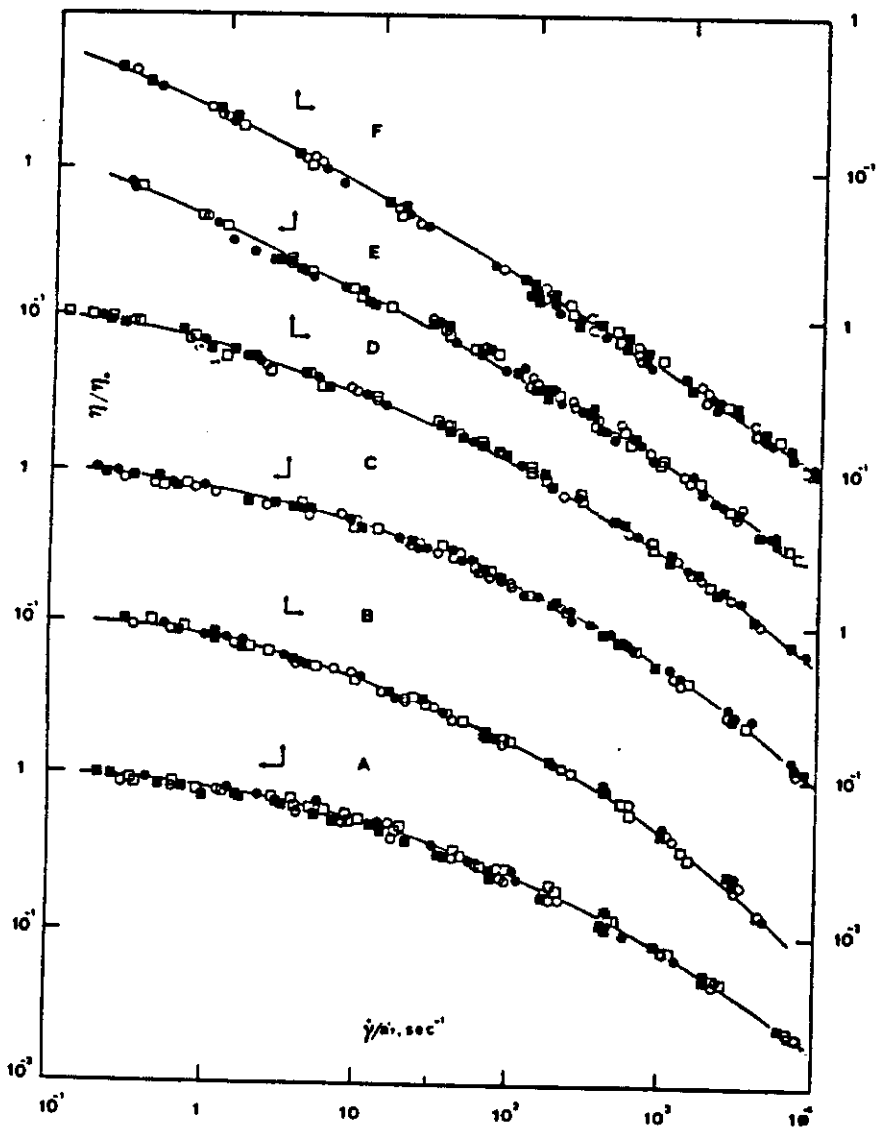

Fig. 13. Generalized dimensionless viscosity curves for each polymer. Key for symbols as in figure 3

Determining the slope n' in the logarithmic plots τ vs. $\dot{\gamma}_{app}$ allows one to perform the Rabinowitch correction for the shear rate [13]:

$$\dot{\gamma} = \dot{\gamma}_{app}\left(\frac{3n'+1}{4n'}\right). \tag{10}$$

In figure 9, the viscosity evaluated through eqs. (9) and (10) is plotted against $\dot{\gamma}$ for all polymers at the temperature of 180 °C. One may note that the zero-shear viscosity has not been attained for samples E and F. In these cases, use has been made of the Ferry's relation to evaluate η_0 [14]:

$$\frac{1}{\eta} = \frac{1}{\eta_0} + b\tau. \tag{11}$$

A good agreement has been found between the values of η_0 obtained in this way and those determined experimentally elsewhere [15] with a cone-and-plate viscometer.

All the η_0 values are shown in figure 10 as a function of the inverse of the absolute temperature. By using the Arrhenius equation:

$$\eta_0 = K_\eta \exp\left(-\frac{E}{RT}\right) \tag{12}$$

it was possible to evaluate the activation energy, E. The values of E have been plotted against $M_w\beta$ (see figure 11) and a simple relationship has been found, of the form:

$$E = -3.385 + 0.73\ln(M_w\beta). \tag{13}$$

Following [16], the best expression for the dependence of the zero-shear viscosity on molecular weight and molecular weight distribution was found to be

$$\ln\eta_0 = -20.55 + 2.75\ln(M_w\beta^{0.152}). \tag{14}$$

The above relationship, specifically found for the data at 180 °C and shown in figure 12, indicates a dependence on both M_w and β smaller than that predicted by various theories [17, 18]. Of course, through eqs. (12) and (13), the relationship (14) can give the zero-shear viscosity for any HDPE sample at any other temperature.

Figure 13 shows the generalized viscosity curves in the form of η/η_0 vs. $\dot{\gamma}/a_T''$, obtained from data at different temperatures. The reference temperature is T_r = 190 °C.

The temperature shift factor for all polymers is given by

$$a_T'' = 1 + K''(T - T_r), \tag{15}$$

where K'' is in turn a function of M_w and β. The experimentally found relationship is

$$K'' = -0.048 + 5\cdot10^{-3}(M_w\beta). \tag{16}$$

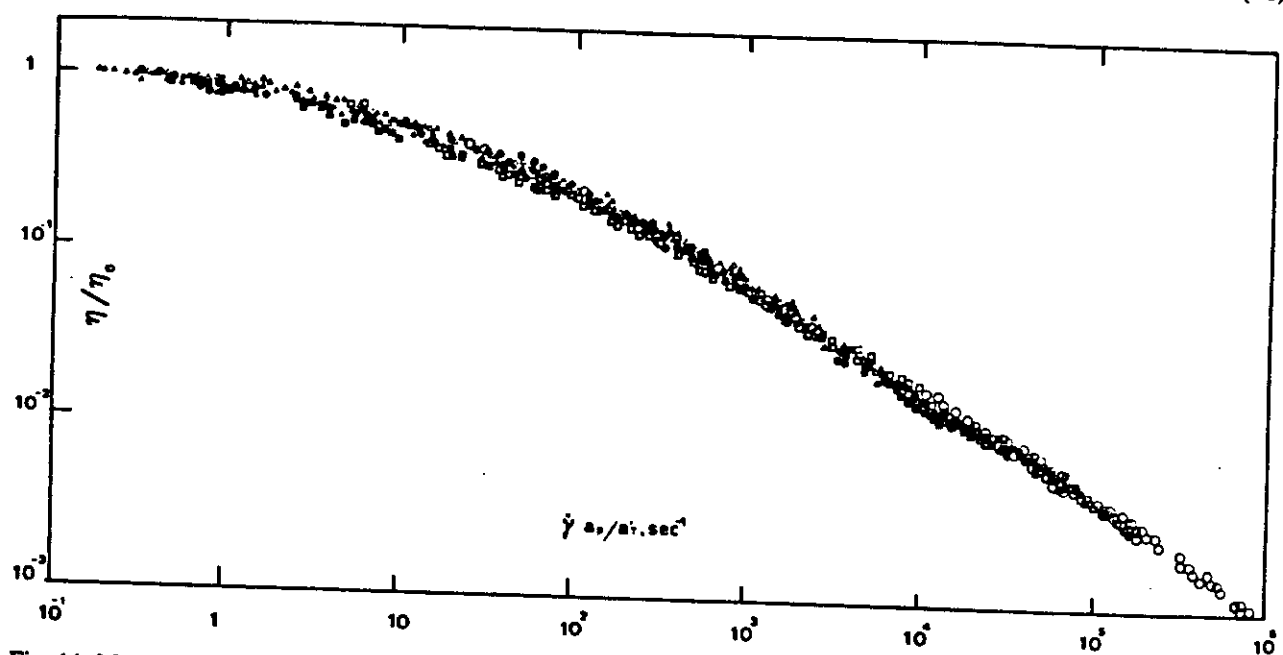

Fig. 14. Master curve for the dimensionless viscosity. Key for symbols as in figure 4

A further superposition has been attempted with the data of figure 13 in order to obtain a single curve for all polymers. A horizontal shift is sufficient to obtain the curve reported in figure 14 with a shift factor which depends on molecular weight and molecular weight distribution through the relationship

$$a_p = 6.95 \cdot 10^{-6} (M_w \beta)^{0.94} . \quad (17)$$

Figure 14, together with eqs. (15–17) determines the ratio η/η_0 for any polymer as well as for any value of shear rate.

4. Concluding remarks

By analysing rheological data obtained on well characterized HDPE samples, generalized relationships have been found for the entrance corrections as a function of temperature, weight-average molecular weight and molecular weight distribution. Furthermore, generalized relationships have been found for the zero-shear viscosity and for the shift factors of the whole viscosity curve. The full set of these results is of technological relevance insofar as it allows one to evaluate not only the viscosity but also the true pressure drop for short capillaries, thus providing useful information for die design.

Acknowledgement

This work was carried out with the financial support of "Progetto Finalizzato del C.N.R. Chimica Fine e Secondaria".

References

1. Middleman, S., "The flow of high polymers", Interscience (New York 1968).
2. Ferry, J. D., "Viscoelastic properties of polymers", J. Wiley (New York 1970).
3. Han, C. D., "Rheology in polymer processing", Academic Press (New York 1976).
4. Kumar, N. G., J. Polym. Sci. Macromolecular Reviews 15, 255 (1980).
5. Bogue, D. C., J. L. White, "Engineering analysis of non-newtonian fluids", Agardograph, NATO Series, 144, 1970.
6. Romanini, D., Montedison, Ferrara (Italy), private communication.
7. Bagley, E. B., J. Appl. Phys. 28, 624 (1957).
8. Van Wazer, J. R., J. W. Lyons, K. Y. Kimm, R. E. Colwell, "Viscosity and flow measurements. A Laboratory Handbook of Rheology", Interscience (New York 1963).
9. Williams, M. L., R. F. Landel, J. D. Ferry, J. Am. Chem. Soc. 77, 3701 (1955).
10. Cogswell, F. N., Polym. Eng. Sci. 12, 64 (1972).
11. White, J. L., A. Kondo, J. Appl. Polym. Sci. 21, 2289 (1977).
12. Han, C. D., M. Charles, Trans. Soc. Rheol. 15, 371 (1971).
13. Rabinowitsh, B., J. Phys. Chem. A 145, 1 (1929).
14. Ferry, J. D., J. Am. Chem. Soc. 6, 1330 (1942).
15. Romanini, D., A. Savadori, Montedison, Ferrara (Italy), private communication.
16. Locati, G. C., L. Gargani, J. Polym. Sci. Polym. Letters Ed. 11, 95 (1973).
17. Graessley, W. W., J. Chem. Phys. 47, 1942 (1967).
18. Saeda, S., J. Yotsuyanagi, K. Yamaguchi, J. Appl. Polym. Sci. 15, 277 (1971).

(Received June 22, 1982)

Authors' address:

Prof. F. P. La Mantia, Dr. A. Valenza, Prof. Dr. D. Acierno
Istituto di Ingegneria Chimica
Università di Palermo
Viale delle Scienze
I-90128 Palermo

Rheologica Acta

Rheol. Acta 22, 308 – 312 (1983)

A comprehensive experimental study of the rheological behaviour of HDPE. II. Die-swell and normal stresses

F. P. La Mantia, A. Valenza, and D. Acierno

Istituto di Ingegneria Chimica, Università di Palermo (Italy)

Abstract: Die-swell data have been obtained for six high-density-polyethylene (HDPE) samples. The data are presented in the form of generalized relationships taking into account both molecular and operational parameters.

Data obtained from annealed samples have been used to calculate the first normal-stress difference by using Tanner's approach. An analytical expression has been found correlating the normal-stress difference with the shear-stress taking into account the molecular characteristics.

Key words: High-density-polyethylene, die-swell, normal stress

1. Introduction

In the first paper of this series [1] we mentioned that the dependence of the rheological characteristics of molten polymers on structural parameters is in many cases not even qualitatively well established [2, 3]. Studying six different high-density-polyethylene samples we considered quantitatively the influence of molecular weight and molecular weight distribution on entrance phenomena and steady-shear viscosity. Generalized relationships were found which may certainly be considered to be of technological importance in die design.

The aim of this paper is to further this study by obtaining diameter data at the exit of a capillary (die-swell) on the same HDPE samples. The data are again presented in the form of generalized relationships taking into account both molecular (molecular weight and molecular weight distribution) and operational (length-to-diameter ratio, temperature, flow rate) parameters. Furthermore, by making use of a well-known thoretical approach [4], some of the results were used to calculate values of the first normal-stress difference which were found to agree well with the literature [5, 6].

2. Experimental

The materials used were the six high density polyethylene samples studied previously, whose molecular characteristics were reported in table 1 of [1].

The tests were performed at four different temperatures (160, 170, 180 and 190 °C) in a constant rate extruder equipped with various length-to-diameter ratios (5, 10, 20 and 40) capillaries. The diameter was always 1 mm and the entrance angle was 90°. The velocity varied from 0.05 cm/min up to the appearance of instability phenomena.

For the diameter measurements samples about 5 cm long were cut to avoid changes in diameter due to their own weight. These measurements were made using a micrometer after the samples had solidified.

The swelling ratio, B, was evaluated as in [7]:

$$B = \frac{D'}{D}(\rho V_m)^{1/3}. \tag{1}$$

In eq. (1) D' is the diameter of the extruded sample, D the die diameter, ρ the density of the polymer at room temperature, and V_m the specific volume at the extrusion temperature. V_m values (in cm^3/g) were obtained, following [8], from the relationship:

$$V_m = 1.1405 + 9.4 \cdot 10^{-4} T^{-1} \tag{2}$$

with T in °C.

The samples extruded through the capillary with a length to-diameter ratio $L/D = 40$ were annealed in silicone oil for about 15 min at 150 °C to obtain stress-free samples [7] and to enable the normal stresses to

be calculated. During the annealing operations neither swelling nor dissolution of the polymeric sample in the oil took place.

The swelling ratio after annealing, B_a, was evaluated using eq. (1) in which of course D' was the diameter measured after annealing and cooling to room temperature.

3. Analysis of the results

Let us first discuss the die-swell results that are more relevant in the processing operations, i.e. those with frozen-in stresses.

Figure 1 shows the swelling ratio, B, for all the polyethylene samples as a function of the shear stress at various L/D. The use of this plot was suggested in [2] as a means of eliminating the temperature dependence and indeed the data obtained at different temperatures are found to fall on the same curve. The dependence of B on the length to diameter ratio is clearly evident with B increasing as L/D decreases. The influence of the capillary length however becomes less and less important as L/D increases.

The data in figure 1 also show that B increases with both the average molecular weight (M_w for instance) and the molecular weight distribution ($\beta = M_w/M_n$), in agreement with the results of Rogers [10] and Romanini [11] but in conflict with the data of Mendelson and Finger [12]. A quantitative dependence on both quantities is found through their product [11] as shown by figure 2, at any L/D and for given shear stresses. A relationship of the type:

$$B = k_B + C_B \ln(M_w \beta) \tag{3}$$

describes the data very well. k_B and C_B depend both on the shear stress and the L/D ratio, and their dependence can be written analytically as:

$$k_B = 13.125 - 0.725\frac{L}{D} + 0.014\left(\frac{L}{D}\right)^2 + \left[-0.99 + 0.584\frac{L}{D} - 1.131 \cdot 10^{-3}\left(\frac{L}{D}\right)^2\right] \cdot \ln\tau, \tag{4}$$

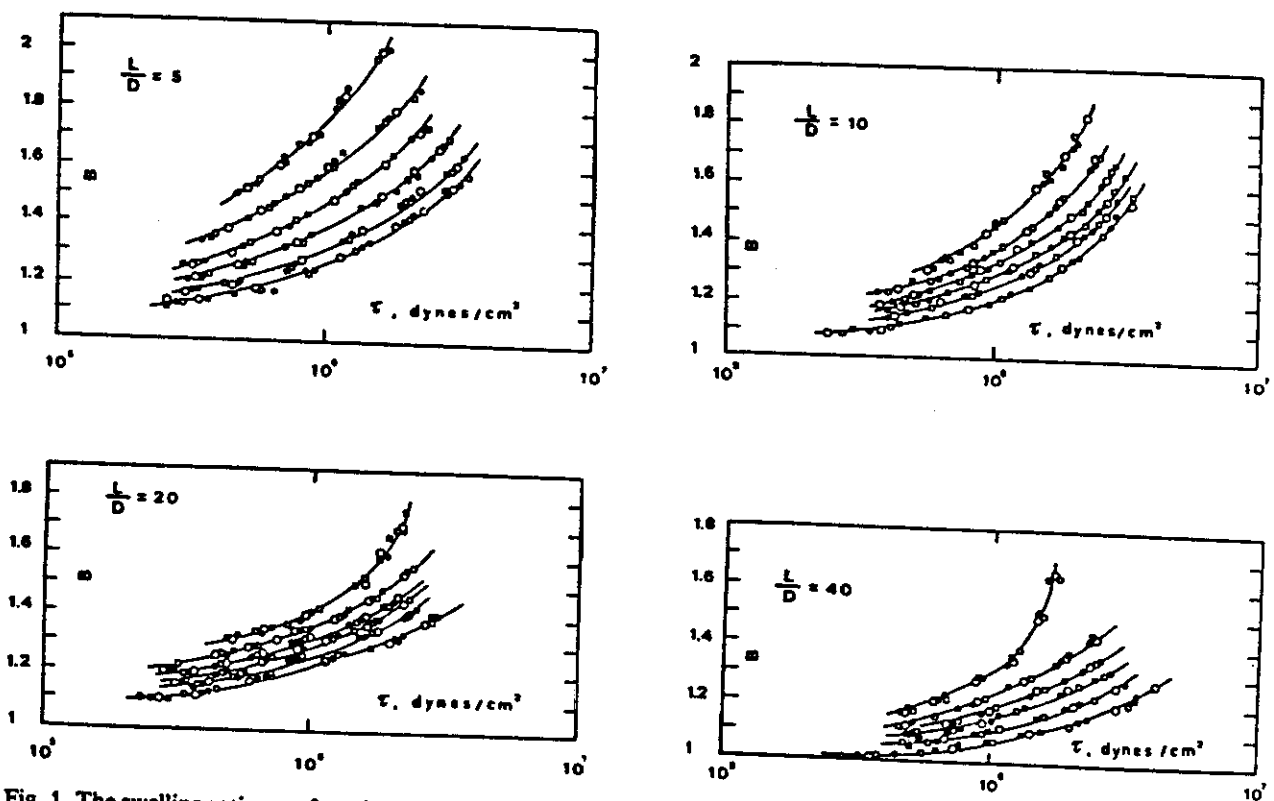

Fig. 1. The swelling ratio as a function of the shear stress for all the samples. Different symbols correspond to different temperatures: ○ – 160°C; □ – 170°C; ● – 180°C; ■ – 190°C. Polymers from top to bottom are: *F, E, D, C, B, A*

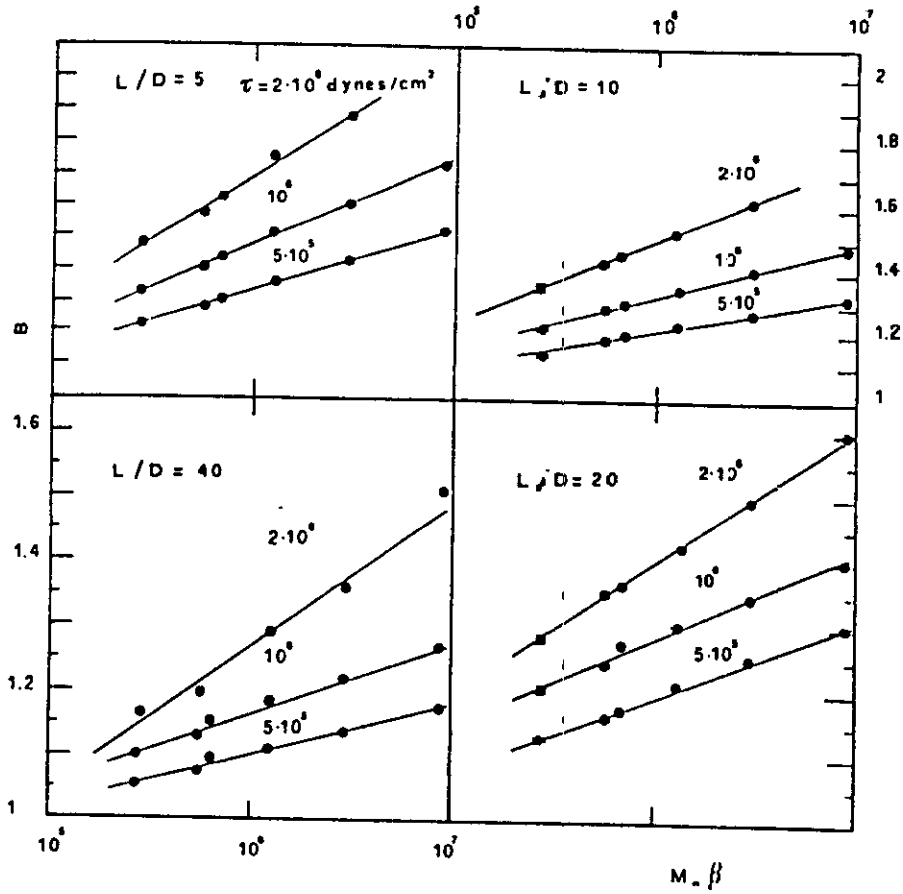

Fig. 2. The swelling ratio as a function of $M_w\beta$ at fixed values of the shear stress and for all the L/D ratios

$$c_B = -1.1416 + 0.0627\frac{L}{D} - 1.182\cdot 10^{-3}\left(\frac{L}{D}\right)^2 + \left[0.0937 - 5.064\cdot 10^{-3}\frac{L}{D} + 9.48\cdot 10^{-5}\cdot\left(\frac{L}{D}\right)^2\right]\ln\tau \qquad (5)$$

where τ is expressed in dynes/cm^2. The correlation factor for both the above expressions is satisfactory (>0.95).

The use of eqs. (3–5) allows one to predict the swelling ratio for any HDPE sample as a function of the geometrical characteristics of the capillary (L/D) and of the operating conditions (either τ or $\dot{\gamma}$ and T with the aid of the previous results [1]). Of course the above expressions can only be used with confidence in the explored range of L/D and shear stress and certainly cannot be extrapolated to cases where $L/D < 1$.

In order to derive values of the first normal-stress difference from die-swell measurements it was necessary to anneal the samples to release the frozen-in stresses, as described in the experimental section. B_a data for $L/D = 40$ are shown in figure 3. It is seen that the swelling ratio after annealing also increases with τ, M_w and β, as found by other researchers [7, 11, 12]. The following evaluation of normal stresses has been restricted to the L/D ratio of 40 for reasons described in the literature [4].

Among the several available theoretical analyses, Tanner's [4] has been chosen both because it can in some sense be considered the more rigorous [2, 13] and because it has already been successfully employed to produce results that agree favourably with independently measurements [13].

The expression used for the calculations was [14]:

$$\sigma = \tau_{11} - \tau_{22} = 2\tau[2(B_a - 0.1)^6 - 2]^{0.5} \qquad (6)$$

where the 0.1 term is, according to Tanner [14], to account for the limiting die swell.

The results are shown in figure 4 as first normal-stress difference vs. shear stress. Qualitatively we may say that, at fixed τ, σ increases with M_w and β in good agreement with results in the literature [9]. Further-

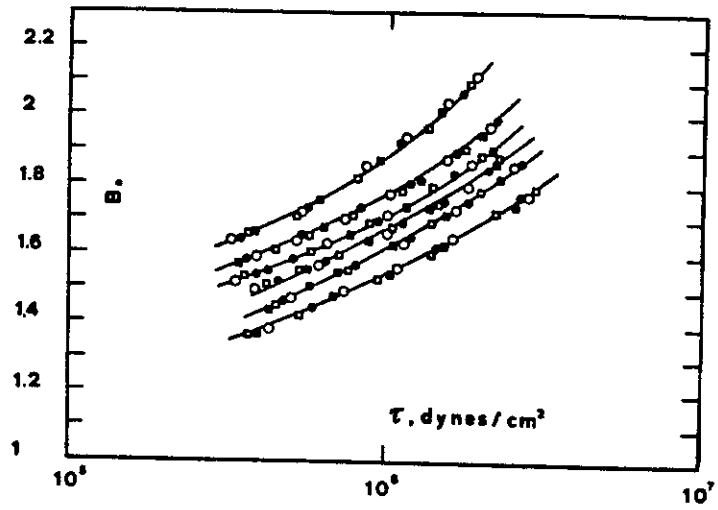

Fig. 3. The swelling ratio after annealing as a function of the shear stress for $L/D = 40$. Symbols as in figure 1

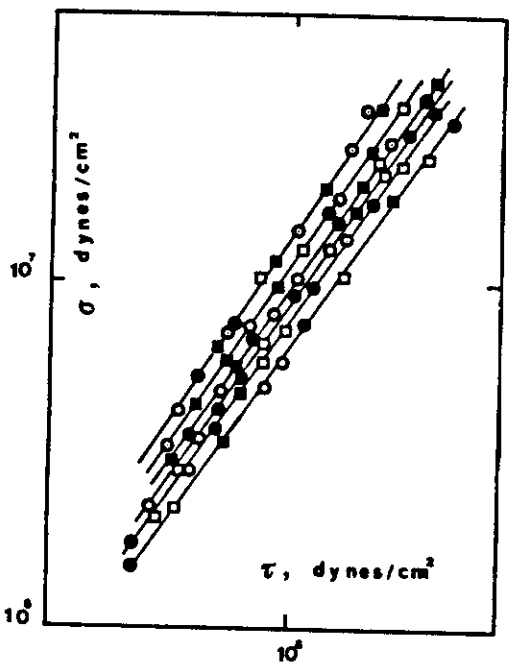

Fig. 4. First normal-stress difference, calculated from eq. (6), as a function of the shear stress. Symbols as in figure 1

more, the slope in the log-log $\sigma - \tau$ plot increases with the molecular weight but does not seem to change with the molecular weight distribution. Quantitatively, for the explored τ range, we may write:

$$\sigma = k_\sigma \tau^{C_\sigma} \tag{7}$$

with

$$k_\sigma = 0.42\, M_w^{-0.324} \tag{8}$$

and

$$C_\sigma = 0.82 + 5.67 \cdot 10^{-2} \ln M_w$$

when τ and σ are given in dynes/cm^2.

4. Concluding remarks

Swelling ratios have been measured for six HDPE samples with frozen-in stresses. The data show an increase of the swelling with both molecular weight and molecular weight distribution. Analytical expressions are found which may be used with high confidence to predict the swelling ratio as a function of the above molecular characteristics, the geometrical characteristics and the operating conditions.

Data taken on annealed samples have been used to derive values of the first normal-stress differences and again an analytical expression has been found correlating the first normal-stress difference with the shear stress taking into account the molecular characteristics. In this case however the influence of M_w seems to predominate over that of β.

Acknowledgement

This work was carried out with the financial support of "Progetto Finalizzato del C.N.R. Chimica Fine e Secondaria".

References

1. La Mantia, F. P., A. Valenza, D. Acierno, Rheol. Acta 22,299 (1983).
2. Han, C. D., "Rheology in Polymer Processing", Academic Press (New York 1976).

3. Bogue, D. C., J. L. White, "Engineering analysis of non-newtonian fluids" Agardograph, NATO Series, 144, 1970.
4. Tanner, R. I., J. Polym. Sci. A 2, 2067 (1970).
5. Han, C. D., T. C. Yu, K. U. Kim, J. Appl. Polym. Sci. 15, 1149 (1971).
6. Shroff, R. N., M. Shida, Trans. Soc. Rheol. 21, 327 (1977).
7. Mendelson, R. A., F. L. Finger, J. Appl. Polym. Sci. 17, 797 (1973).
8. Hunter, E., W. G. Oakes, Trans. Faraday Soc. 41, 49 (1945).
9. Han, C. D., J. Appl. Polym. Sci. 15, 2567, 2579 (1971).
10. Rogers, M. G., J. Appl. Polym. Sc. 14, 1679 (1970).
11. Romanini, D., A. Savadori, G. Giarotti, Polymer 21, 1092 (1980).
12. Mendelson, R. A., F. L. Finger, J. Appl. Polym. Sci. 19, 1061 (1975).
13. Racin, R., D. C. Bogue, J. Rheol. 23, 263 (1979).
14. Tanner, R. I., Appl. Polym. Symp. 20, 201 (1973).

(Received June 7, 1982)

Authors' address:

Prof. F. P. La Mantia, Dr. A. Valenza, Prof. Dr. D. Acierno
Istituto di Ingegneria Chimica
Università di Palermo
Viale delle Scienze
I-90128 Palermo

Rheologica Acta

Rheol. Acta 21, 452 – 455 (1982)

Extensional flow of HDPE/LDPE blends

F. P. La Mantia, D. Acierno, and D. Curto

Istituto di Ingegneria Chimica, Università di Palermo

Abstract: Elongational viscosity data, obtained through the converging flow analysis by Cogswell, are presented for two types of HDPE/LDPE blends at various compositions and different temperatures. The results relative to the homopolymer parents compare favourably with literature data obtained also with different and more sophisticated techniques. Those relative to blends show peculiar features for the two cases: when the newtonian viscosity of the LDPE is higher all the blends show a behaviour typical of the LDPE with a maximum in η_{el}/η_0 enhanced at small percentage of HDPE; when the newtonian viscosity of the LDPE is similar to that of the HDPE there is only a gradual change in the properties.

Key words: Elongational viscosity, converging flow, polymer blend

1. Introduction

Extensional flow of polymer melts has recently received more and more attention [1 – 3] due to its implications in many technological processes such as fiber spinning, film blowing, etc. However the techniques adopted to study this flow are often very lengthy and difficult; therefore the data, especially as steady-state values are concerned, are sparse and sometimes contradictory [1, 2, 4 – 6]. The situation is particularly difficult in the field of polymer blends for which data are available only in [7], in spite of the increasing relevance that such materials are gaining [8].

In this work the converging flow analysis by Cogswell [9] has been employed to evaluate the extensional viscosity of HDPE/LDPE blends, which may be considered of interest in the production of thought blown films.

2. Experimental

The materials employed in this work were commercially available high density and low density polyethylenes manufactured and kindly supplied by Solvay (HDPE) and Montedison (LDPE). The MFI of the samples are reported in table 1.

Table 1

Sample code	M.F.I.
HDPE-1	4.90
HDPE-2	0.98
LDPE-2	0.74
LDPE-3	0.07

Two types of blends (HDPE-1/LDPE-3 and HDPE-2/LDPE-2) with various compositions of 20, 40, 60, 80 weight percentage of LDPE were prepared by melt mixing the homopolymers parents in a laboratory mixer (Rheocord, Haake) at 210 °C at about 20 rpm. The mixing time was approximately 20 min, sufficient to obtain in all cases steady-state temperature and torque. The homopolymers were also subjected to the same procedure.

3. Rheological characterization

A constant-force viscometer and a constant-rate viscometer have been employed for determining the rheological characteristics of both the blends and the polymer parents: more precisely the former has been used in the low shear-rate region and the latter in the high shear-rate region.

Three different capillaries have been adopted in all cases: the diameter was always 1 mm and the length to diameter ratios were 40, 10 and 5; the entrance angle was 90°.

The test temperatures have been 160, 180 and 200 °C.

4. Analysis of results and discussion

Following the analysis of Cogswell [9], the elongation viscosity can be found through the relation:

$$\eta_{el} = \frac{9}{32}(n+1)^2 \frac{\Delta P_{ent}^2}{\dot{\gamma}^2 \eta} \tag{1}$$

where ΔP_{ent} is the loss pressure due to the entrance effect, $\dot{\gamma}$ is the apparent shear rate $32Q/D^3$, η the shear viscosity and n the slope in the log-log shear stress-shear rate plot.

The stretching rate is

$$\dot{\varepsilon} = \frac{4}{3(n+1)} \eta \frac{\dot{\gamma}^2}{\Delta P_{ent}} . \tag{2}$$

It is generally considered that ΔP_{ent} can be found by extrapolating a straight line to $L/D = 0$ in a ΔP vs. L/D plot. It is however true [10] that the so found value, is the sum of both entrance and exit pressure losses:

$$\Delta P_{ends} = \Delta P_{ent} + \Delta P_{exit} . \tag{3}$$

It has been further shown that ΔP_{ends} is proportional to the principal normal stress difference [11], and ΔP_{exit} is the sum of the first and second normal stress difference [12], so that

$$\Delta P_{ends} = \alpha \sigma_{11} , \tag{4}$$

$$\Delta P_{exit} = \sigma_{11} + \sigma_{22} . \tag{5}$$

The value of α has been found $\simeq 2$ for many polymers [11], and σ_{22} is a negative fraction of σ_{11}

$$\sigma_{22} = -\varepsilon \sigma_{11} \tag{6}$$

where ε is between 0 and 0.6 [12, 13].

Shortly from eqs. (3) – (6):

$$\Delta P_{ent} = \frac{\alpha - 1 + \varepsilon}{\alpha} \Delta P_{ends} . \tag{7}$$

The value of ε is very uncertain, and however in accordance with Han [14] we have taken the values of 0.4 and 0.5 for LDPE and HDPE respectively. For want of experimental data relative to the blends we have considered for ε a weighted average of the values of the polymer parents.

With the above assumption, from the ΔP_{ends} values taken in the ΔP vs. L/D plots, ΔP_{ent} have been evaluated through eq. (7). With these values and the rheological characteristics of the same blends already reported in [14], η_{el} and $\dot{\varepsilon}$ have been evaluated. Figures 1 and 2 show such data for both types of blend at

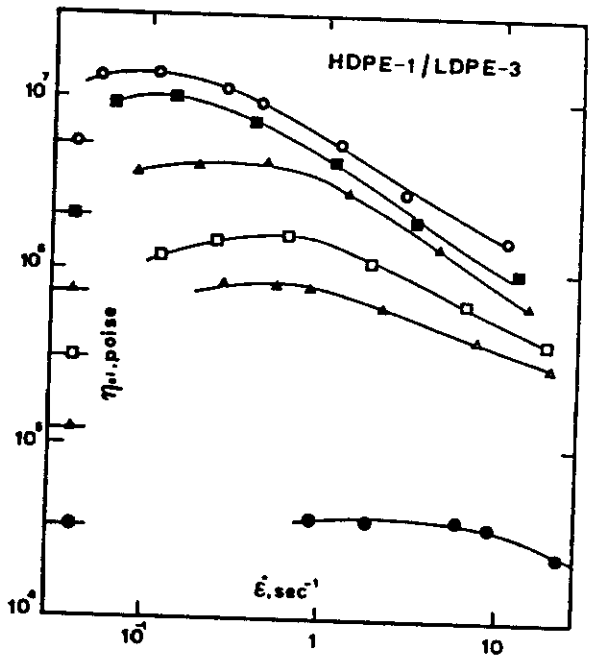

Fig. 1. Elongational viscosity vs. stretching rate for HDPE-1/LDPE-3 at 180 °C. ○ LDPE, ■ 80% LDPE, ▲ 60% LDPE, □ 40% LDPE, △ 20% LDPE, ● HDPE

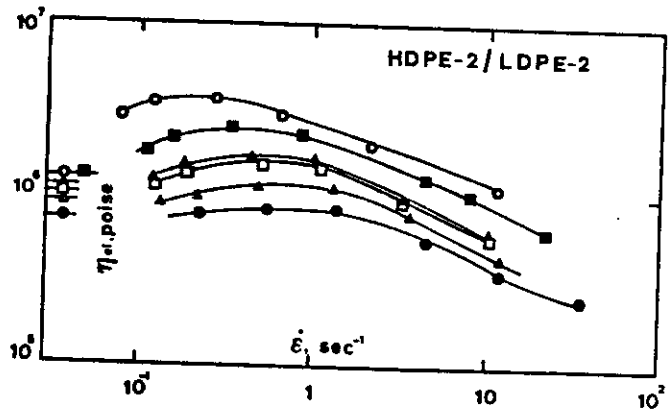

Fig. 2. Elongational viscosity vs. stretching rate for HDPE-2/LDPE-2 at 180 °C. Key for symbols as in figure 1

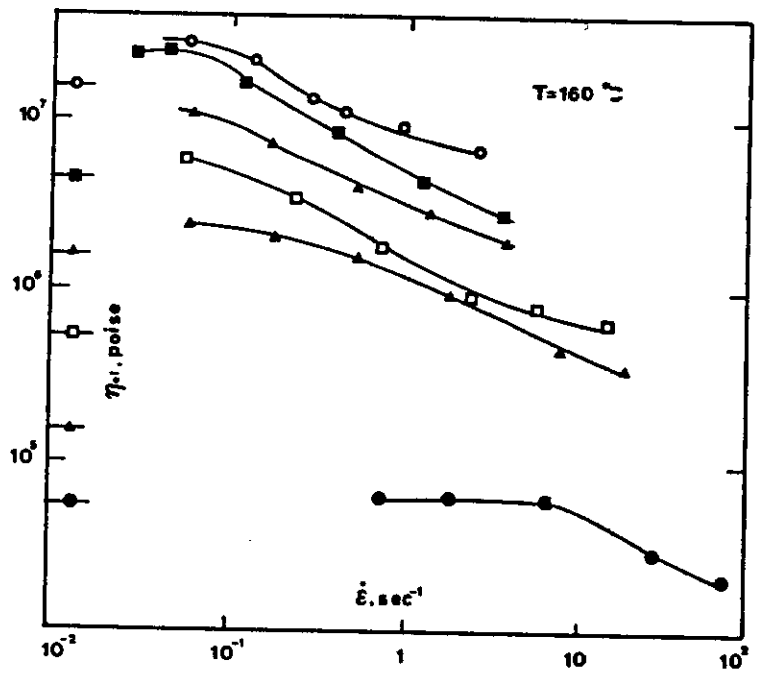

Fig. 3. Elongational viscosity vs. stretching rate for HDPE-1/LDPE-3 at 160 °C. Key for symbols as in figure 1

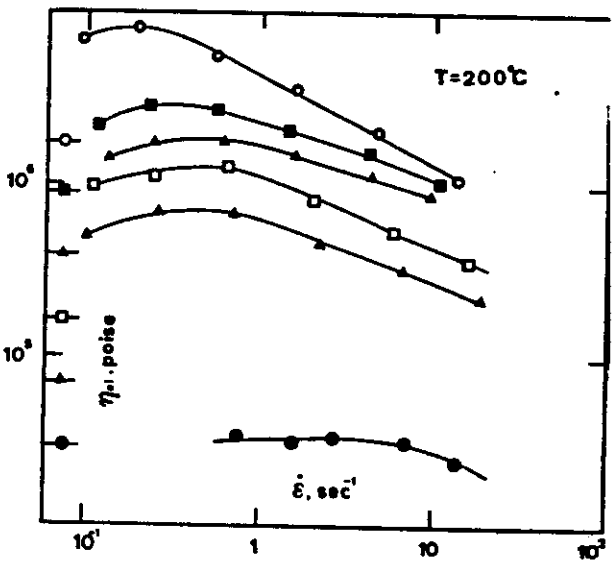

Fig. 4. Elongational viscosity vs. stretching rate for HDPE-1/LDPE-3 at 200 °C. Key for symbols as in figure 1

T = 180 °C. Figures 3 and 4 further show data for HDPE-1/LDPE-3 at 160 and 200 °C respectively. In all cases the Trouton value $3\eta_0$ has been reported in the figures for comparison.

The curves relative to the pure LDPE show n all cases a significant maximum whose value, relative to the Trouton viscosity, increases when η_0 decreases. Also a shif of the maximum toward higher stretching rates is evident decreasing the Trouton value.

The data of the HDPE show only a very slight maximum in the case of HDPE-2, which has a higher viscosity. All these features are in good agreement with literature results [4].

The viscosities of the blends lie for all the cases between those of the pure polymers. However there are typical features peculiar of each type of mixture. When the shear viscosity of the LDPE is much higher than that of the HDPE, all blends show a behaviour very similar to that of the low density polyethylene and the ratio $\eta_{el}/3\eta_0$ becomes much larger increasing the HDPE content. This unexpected result is probably due to the fact that the blend behaves like a LDPE with a lower molecular weight. The shift of the maximum toward higher stretching rates seems to confirm this hypothesis.

The system HDPE-2/LDPE-2 with similar newtonian viscosities, shows a gradual change from one type of behaviour to another, and indeed, when the concentration of the high density polyethylene is 80%, the maximum almost disappears.

Such a behaviour can be explained with the hypothesis that in this case, where the molecular weights of the two homopolymers are not too different, the primary effect is on the average a decrease in the degree of branching with increasing HDPE content.

Qualitatively figures 3 and 4 confirm the above indication with the obvious quantitative differences

due to the temperature (and therefore newtonian viscosity) variations. The same features are present also in the data at different temperatures for the system HDPE-2/LDPE-2 not reported here.

This work has been carried out with the financial support of "Progetto Finalizzato del C.N.R. Chimica Fine e Secondaria".

References

1. Cogswell, F. N., Appl. Polym. Symp. 27, 1 (1975).
2. White, J. L., Appl. Polym. Symp. 33, 31 (1978).
3. Petrie, C. J. S., Elongational Flow, Pitman (London 1979).
4. Münstedt, H., Joint Meeting of British, Netherlands and Italian Societies of Rheology (Pisa 1977).
5. Laun, H. M., H. Münstedt, Rheol. Acta 17, 415 (1978).
6. Raible, T., A. Demarmels, J. Meissner, Polymer Bulletin 1, 397 (1979).
7. Cogswell, F. N., Trans. Soc. Rheol. 16, 383 (1972).
8. Paul, D. R., S. Newmann (eds.), Polymer Blends, Academic Press (London 1978).
9. Cogswell, F. N., Polym. Eng. Sci. 12, 64 (1972).
10. Han, C. D., Rheology in Polymer Processing, Academic Press (London 1976).
11. White, J. L., A. Kondo, J. Appl. Polym. Sci. 21, 2289 (1977).
12. Han C. D., Trans. Soc. Rheol. 18, 163 (1974).
13. Lee, B. L., J. L. White, Trans. Soc. Rheol. 18, 467 (1974).
14. Curto, D., D. Acierno, F. P. La Mantia, submitted for publication.

(Received April 15, 1982)

Authors' address:

Dr. F. P. La Mantia, Prof. D. Acierno, Dr. D. Curto
Istituto d Ingegneria Chimica
Universita di Palermo
Viale delle Scienze
I-90100 Palermo

Plastics and Rubber Processing and Applications 5 (1985) 183-188

Short communication

The rheological behaviour of HDPE/LDPE blends. III. Melt strength and extensibility

Abstract: Melt strength (MS) and breaking stretching ratio (BSR) data of some HDPE/LDPE blends are given.

Some peculiarities are shown when one looks at the values of MS and BSR as a function of the composition: more particularly a large synergistic effect and an antagonistic effect are shown by the melt strength and the breaking stretching ratio data, respectively. This suggests the possibility of employing some blends instead of the homopolymers to obtain easier processing.

1 Introduction

The blending of polymers is a very important route for obtaining materials with *ad hoc* tailored properties, both in the solid state and during melt processing. The rheological properties of the polymer blends play an important role. Nevertheless, only a few experimental indications rather than general theoretical considerations are present in literature.[1-3]

Polyolefine blends, and in particular blends of various polyethylenes, are of remarkable interest in view of the production of transparent tough films,[1-4] but their rheological characterization is still lacking, although a number of papers have been devoted to this subject.[5-9]

More particularly, elongational data relative to these systems are certainly scarce and only one paper deals extensively with this subject.[10] In that paper, however, the extensional behaviour is investigated by means of the theoretical treatment of shear data.

The aim of the work reported is to study the non-isothermal tensile behaviour of HDPE/LDPE blends in spinning experiments by using a new melt tension tester already presented.[11,12]

Although much more difficult to interpret from a scientific point of view and to correlate to other rheological characteristics, non-isothermal tensile data appear interesting both because they can be obtained quite readily, experimentally, and especially because the processing operations for which elongational flow is relevant (fibre spinning, film blowing) are performed under non-isothermal conditions.

2 Experimental

The materials employed were commercially available high-density and low-density polethylenes, manufactured and kindly supplied by Solvay and Wacker (HDPE) and Montedison (LDPE). In the following, the samples will be indicated as HDPE-X and LDPE-X with X increasing as the Melt Flow Index decreases (see Table 1).

Table 1. Samples used

Sample code	MFI
HDPE-2	0·98
HDPE-4	0·11
LDPE-1	3·90
LDPE-2	0·74

Two types of blends were prepared: HDPE-2/LDPE-2 and HDPE-4/LDPE-1. The blends of the first type have already been completely characterized in shear flow[8,9] and some in extensional flow.[10] The system HDPE-4/LDPE-1 is different from those previously studied, but its behaviour in shear is very similar to that of the blends HDPE-3/LDPE-1 of the previous papers.[8,9] In both cases, one of the polymer parents (LDPE-2 and HDPE-4) is used for film blowing while the other polyethylene has a viscosity too low to use in this technological operation.

Various compositions have been considered in all cases: more particularly the values of the weight percentage of LDPE, φ, were 0, 20, 40, 60, 80, 100.

The blends were prepared by melt mixing the polymer parents in a laboratory mixer (Plasticorder Brabender model PLE 330) at 210°C and 20 rev min^{-1}. The mixing time was approximately 20 min, sufficient to obtain steady-state conditions for temperature and torque in all cases. The homopolymers were also subjected to the same procedure.

All the experimental runs were carried out on a new capillary rheometer, a Rheoscope 1000, manufactured by CEAST (Turin, Italy), equipped with a tensile module. Here, the extruded monofilament passes through a pulley system and is then drawn by two counter-rotating rolls. The run is carried out by pulling the monofilament, extruded at a given flow-rate Q, at a rotational speed which increases with a linear acceleration of 1 rev min^{-1} s^{-1}. The test ends with the breaking of the filament.

The force in the molten filament at breaking is read directly and is known as melt strength. The breaking stretching ratio was calculated as the ratio between the drawing speed and the extrusion velocity at the die.

All the data were collected at an extrusion temperature of 180°C; the capillary employed was 1 mm in diameter, with $L/D = 10$ and a flat entry.

Plastics and Rubber Processing and Applications 0144-6045/85/$03.30
Printed in Great Britain

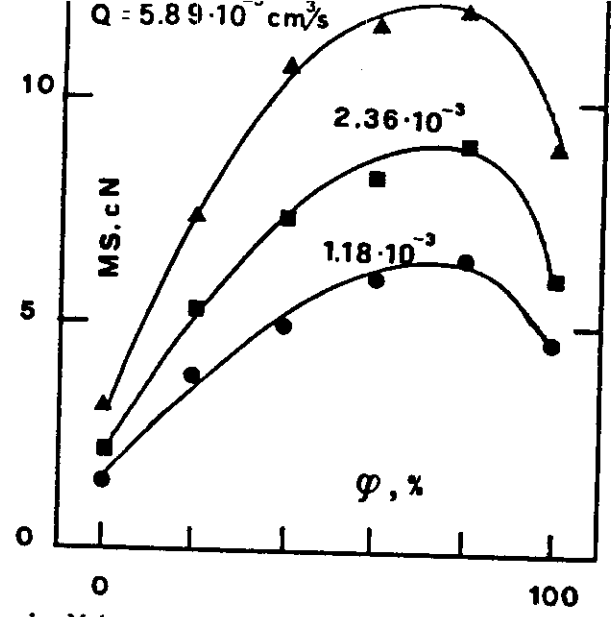

Fig. 1 Melt strength as a function of the blend composition at fixed flow rate for the system HDPE-2/LDPE-2. φ is the weight percentage of LDPE in the blend.

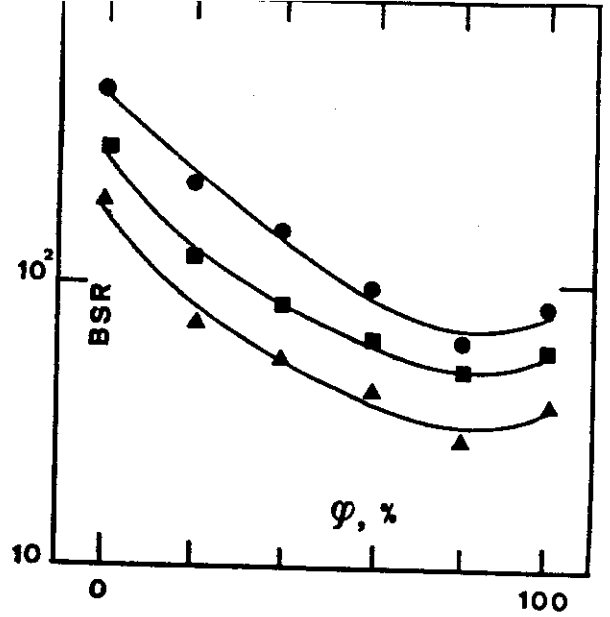

Fig. 3 Breaking stretching ratio as a function of the blend composition at fixed flow rate for the system HDPE-2/LDPE-2. Key of symbols as in Fig. 1.

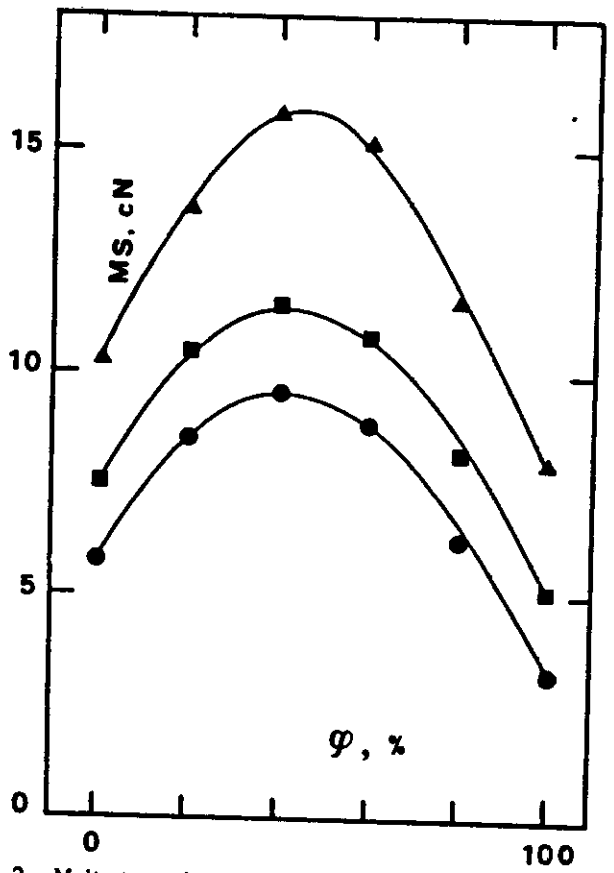

Fig. 2 Melt strength as a function of the blend composition at fixed flow rate for the system HDPE-4/LDPE-1. Key of symbols as in Fig. 1.

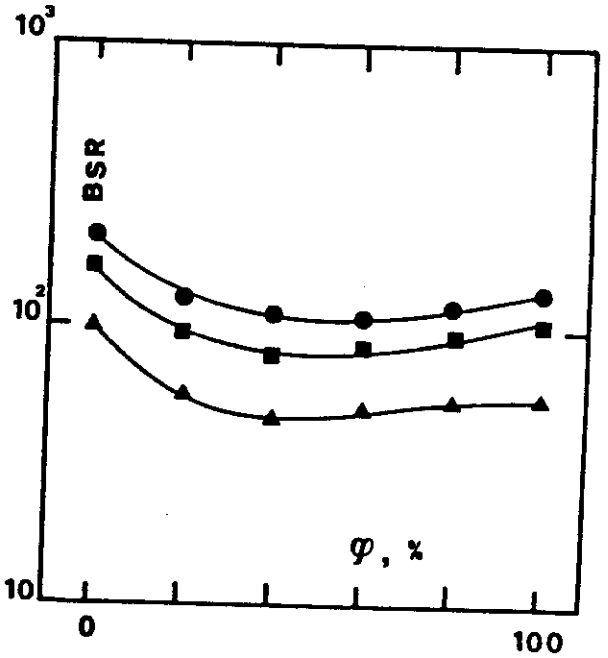

Fig. 4 Breaking stretching ratio as a function of the blend composition at fixed flow rate for the system HDPE-4/LDPE-1. Key of symbols as in Fig. 1.

3 Results and discussion

Figures 1–4 represent the melt strength and the breaking stretching ratio values for all the samples as a function of the blend composition, with the flow rate as parameter.

For both blends a large synergistic effect is shown by the melt strength, but the maximum is present at different compositions and, in particular, is nearer to the homopolymer having the higher melt strength.

On the contrary, an antagonistic effect is shown by the breaking stretching ratio which shows a minimum mostly at the same composition as the maximum in the MS–φ curve.

Now, recall that a polymer can be processed

easily in a film blowing operation when it has an elevated melt strength to sustain the mechanical stress due to the process and a high extensibility in order to achieve the desired thickness. For this reason the polyethylenes used in film blowing processes are low MFI polymers such as HDPE-4 and LDPE-2 among high density and low density polyethylenes, while HDPE-2 and LDPE-1 have melt strength values too low to be used as film blowing materials.

It seems possible, from the above data, that blends of these polyethylenes having high MFI with film blowing grades of polyethylene can give rise to materials with a convenient melt strength and with a breaking stretching ratio not significantly reduced.

In particular, one may employ in the film blowing process either HDPE (HDPE-2) samples with MFI values larger than those usually considered (HDPE-4) by adding small amounts of LDPE, especially because of the increase in MS, or LDPE samples with a rather low viscosity (LDPE-1) with some quantity of HDPE with a low MFI obtaining BSR values that are not too small and high melt strength values. Of course, because these blends have a lower viscosity than that of film blowing grades they are easier to process and an interesting energy saving is also obtained.

Acknowledgement

This work has been carried out with the financial support of Progetto Finalizzato del CNR Chimica Fine e Secondaria.

Thanks are due to Istituto per la Chimica e la Tecnologia dei Materiali Polimerici for allowing us to use the Rheoscope 1000 and to CEAST for allowing use of the tensile module.

References

1. PLOCHOCKI, A. P. In: *Polymer blends*, Paul, D. R. and Newmann, S. (eds.), Vol. 2, Academic Press, New York, 1978, p. 319.
2. HAN, C. D. *Multiphase flow in polymer processing*, Academic Press, New York, 1981.
3. UTRACKI, L. A. and KAMAL, M. R. *Polym. Engng. Sci.*, 22 (1982), p. 96.
4. Japar Patent No. J4.9064667, 1974; West Germany Patent No. 2304998, 1973.
5. PLOCHOCKI, A. P. *Polym. Engng. Sci.*, 22 (1982), p. 1153.
6. DOBRESCU, V. In: *Rheology*, Astarita, G., Marrucci, G. and Nicolais, L. (eds.), Vol. 2, Plenum Press, New York, 1980, p. 555.
7. JACCVIC, M. S., POLLOCK, D. and PORTER, R. S. *J. Appl. Polym. Sci.*, 23 (1979), p. 517.
8. CURTO, D., LA MANTIA, F. P. and ACIERNO, D. *Rheol. Acta*, 22 (1983), p. 197.
9. LA MANTIA, F. P., CURTO, D. and ACIERNO, D. *Acta Polym.*, 35 (1984), p. 71.
10. LA MANTIA, F. P., ACIERNO, D. and CURTO, D. *Rheol. Acta*, 21 (1982), p. 452.
11. LA MANTIA, F. P. and ACIERNO, D. *European Meeting on Polymer Processing and Properties*, Capri, Italy, June 1983.
12. LA MANTIA, F. P. and ACIERNO, D. *Polym. Engng. Sci.* (in press).

F. P. La Mantia and D. Acierno

Istituto di Ingegneria Chimica,
Università di Palermo,
Italy

(Received: 19 July 1984)

Flow Properties of Low Density/Linear Low Density Polyethylenes

D. ACIERNO

Istituto di Ingegneria Chimico-Alimentare
University of Salerno
Salerno, Italy

and

D. CURTO, F. P. LA MANTIA, and A. VALENZA.

Istituto di Ingegneria Chimica
University of Palermo
Palermo, Italy

Rheological data have been collected both in shear and non-isothermal elongational flow on three different types of blends, made from one low density polyethylene sample and three linear low density polyethylene samples.

In addition to the flow curves, data are presented on the extrudate-swell phenomenon, on the instability arising in capillary flow and on the tensile behavior in the molten state.

INTRODUCTION

The rheological behavior of polymer blends has in recent years been widely studied in view of the growing interest in such systems and in view of the relevance to processing (1–16). Of course, the flow properties of blends may heavily depend on the mutual compatibility in the molten state of the parent polymers, which in turn should depend on their structure.

Following a rather complete study of the rheology of high density polyethylene/low density polyethylene blends, HDPE/LDPE, (13–15) the aim of this work is to present a set of data on blends obtained by melt mixing linear low density polyethylene, LLDPE, and low density polyethylene samples. From a fundamental point of view it is interesting to evaluate the influence of LLDPE short chain branches, and from an applications viewpoint the data are of great importance because of the possibility of employing such blends in the preparation of improved films without drastic changes in processing equipment and conditions.

Data have been collected both in shear and (non-isothermal) elongational flow on three different types of blends, made from one low density polyethylene sample and three linear low density polyethylene samples. Particular emphasis has been given to the more relevant aspects of the applications, and thus, in addition to the viscosity curves, data are presented on the extrudate-swell, on the instabilities arising in capillary flow, and on the tensile behavior in the molten state.

EXPERIMENTAL

Three samples of LLDPE, polymerized with 1-butene as comonomer and already characterized both from a physico-chemical and a rheological point of view (17), and one sample of LDPE also previously considered (18) have been employed in the preparation of blends.

In the following the samples will be indicated as LD and LL instead of LDPE and LLDPE. The nomenclature of the LL samples will comprise the approximate indication of the melt flow index (*MFI*). The main physico-chemical characteristics of the samples are listed in *Table 1*.

The density, ρ, was measured at 23°C, according to the ASTM-D-1505/68 method. The melt flow index, *MFI*, was evaluated according to the ASTM-D-1238/73 method, procedure B, with a CEAST apparatus. The weight average molecular weight, M_w, and the dimensionless polydispersity, $\beta = M_w/M_n$, were determined by GPC in o-dichlorobenzene, ODCB, at 135°C, with a Waters instrument.

Blends from each LLDPE and LDPE have been prepared at various LDPE content, φ. In all cases the polymers have been mixed for about 20 min at 20 rpm and 210°C in a Brabender Plasticorder equipped with a cam mixer. The torque values have been recorded at the end of the mixing runs.

Rheological measurements in shear flow were carried out in the low shear rate region with the aid of a rotational viscometer in a cone and plate mode (Rheotron, Brabender) and in the high shear rate region with the aid of a constant rate capillary viscometer (Rheoscope 1000, CEAST). For the former apparatus, cone and plate were 5 cm in diameter and the cone angle was 2°; for the latter apparatus a flat entry capillary with D = 1 mm and L/D = 40 was used in most of the cases. For one type of blend (LL0.5/LD) three different capillaries were used in order to evaluate the entrance and exit effects: the diameter was always 1 mm and the length to diameter ratios were 40, 20, and 10. All the above tests were performed at 180°C.

Extrudate samples, cooled to room temperature, about 5 cm long, were cut for diameter measurements which were made by means of a micrometer after solidification of the samples.

The swelling ratio, B, has in all cases been evaluated as (19):

$$B = \frac{D'}{D}(\rho v_m)^{1/3} \qquad (1)$$

where D' is the diameter of the extruded samples, D the die diameter, ρ is the density of the polymer at room temperature, and v_m the specific volume at the extrusion temperature.

Visual observation of the collected samples has been done in order to evaluate the critical parameters, i.e., the shear rate and the shear stress at which the extrudates appear irregular, even only superficially. In most cases this corresponds to the sharkskin in the LD rich samples or to the periodical swelling accompanied by pressure fluctuations in the LL rich samples.

Non-isothermal elongational experiments were carried out, also with the aid of the Rheoscope 1000, equipped with the tensile module. In this mode the extruded monofilament passes through a pulley system and is then drawn by two counter-rotating rolls, the rotational speed of which can be continuously varied with a linear acceleration of 1 rpm/s.

The melt strength, MS, the force in the molten filament at breaking, is directly read. The breaking stretching ratio, BSR, can be calculated as the ratio between the drawing speed at break and the extrusion velocity at the die. The extrusion temperature was 180°C. The capillary employed was the one with an L/D = 10 and the tensile system was situated 25 cm below the die.

RESULTS AND DISCUSSION

Let us first discuss the entrance and exit effects in the capillary, studied for the LL0.5/LD blends, containing the most viscous linear low density polyethylene.

Figure 1 represents the end correction or Bagley's factors, e, evaluated in the usual way (20), as a function of the shear stress τ. One notices that the correction factors of the blends lie between the values of the parent polymers: at low shear rates the e values for the blends are similar to those of the LL0.5 sample rather rapidly increasing with τ as evident especially for the LD rich blends.

On the basis of the above results and of the large L/D ratio used, one may hypothesize that neglecting e values for the other blends (LL1/LD and LL4/LD) should imply minor errors in viscosity evaluations and, as will be apparent in the following, should be of no consequence in the qualitative observations of the present work.

Before presenting and commenting on the viscosity curves let us also say, again with reference to the capillary data, that the Rabinowitch correction to the shear rate has also been performed (21).

The viscosity data are reported in *Figs. 2* to *4* as a function of the shear rate. One may observe that in the low shear rate region, the low density

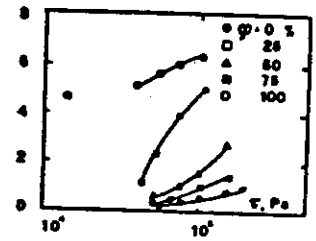

Fig. 1. End correction factor as a function of the shear stress.

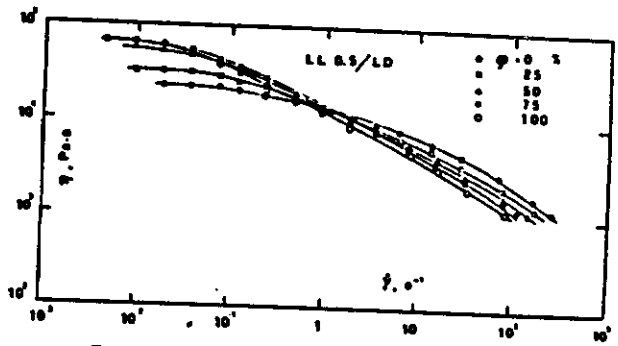

Fig. 2. Flow curves for the LL0.5/LD blends.

Table 1. Physico-Chemical Properties of the Raw Materials.

Resin	Sample code	Density (kg/m³)	M.F.I. (g/10 min)	$M_w \cdot 10^{-3}$	M_w/M_n
LDPE	LD	925	0.27	310	7.3
LLDPE	LL0.5	922	0.53	167	4.7
LLDPE	LL1	924	1.10	136	4.2
LLDPE	LL4	938	4.30	87	4.3

polyethylene has values larger than those of all the linear low density polyethylene samples. However, due to the typically different dependency of the viscosity on the shear rate for the two polymers, the flow curves cross at different $\dot{\gamma}$ values. For LL4/LD this occurs at the shear stress at which the irregularities appear. As for the blends, one may say that in the low shear rate region their viscosity values are mostly between those of the pure polymers. The observations at higher $\dot{\gamma}$ values were rather difficult.

To better elucidate the composition dependence, the viscosities have been also plotted vs. φ on a semilogarithmic scale, at constant stress values (see *Figs.* 5 to 7). The behavior of LL0.5/LD and LL1/LD qualitatively is similar. In both cases, at low stresses the LD has higher viscosity than the LL samples with the values for the blends in between. The variation of η is neither linear nor exponential with φ; in both cases the opposite is also true at the highest stresses, i.e., LD has the lowest viscosity and no simple dependency with φ is seen. In the intermediate τ region the viscosities of the parent polymers are similar and a maximum is present at about φ = 75 percent. As for the LL4/LD system only two cases are present and again a synergistic effect is evident at high stress, when the viscosities of the parent polymers are similar while intermediate viscosity values are shown by the blends at lower stresses when LD has a significantly higher viscosity. Similar observations have previously been made with regard to the

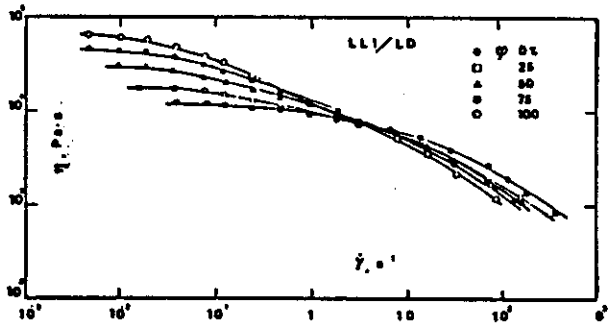

Fig. 3. Flow curves for the LL1/LD blends.

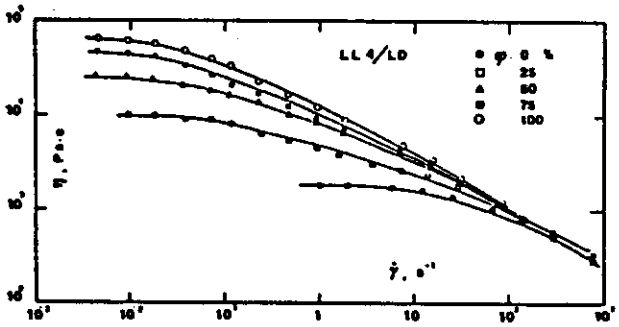

Fig. 4. Flow curves for the LL4/LD blends.

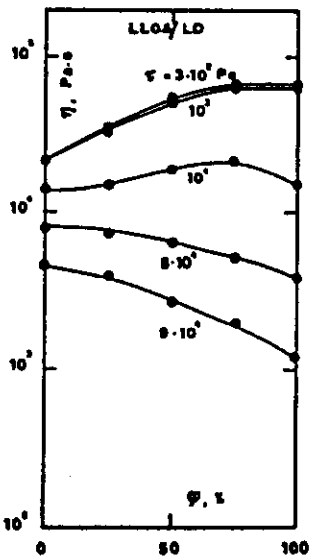

Fig. 5. Viscosity as a function of the composition for the LL0.5/LD blends at fixed constant stress.

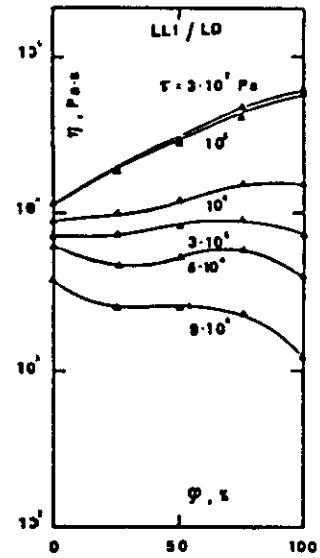

Fig. 6. Viscosity as a function of the composition for the LL1/LD blends at fixed constant stress.

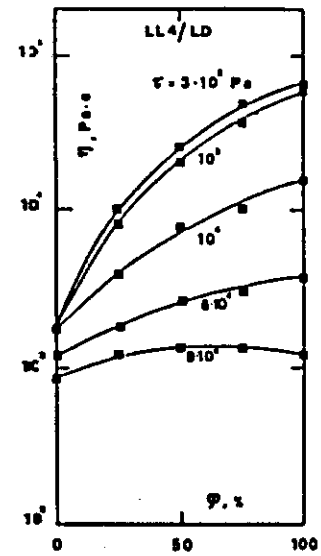

Fig. 7. Viscosity as a function of the composition for the LL4/LD blends at fixed constant stress.

high density polyethylene/low density polyethylene systems (13). We must recall also that the torque values recorded during the preparation of the discussed blends, and reported in *Fig. 8*, show a synergistic effect only in the case of values similar to those of the parents (17).

The swelling results which should not be considered of course as truly rheological data are, however, indicative of elastic effects in the polymer. In particular, *Fig. 9* represents B *vs.* φ at two different τ values for all the systems. All the blends show B values larger than the parent polymers and the effect is of increasing importance going from the LL0.5 to the LL4.

Figure 10 and *11* summarize the results on the appearance of irregularities in the extrudate. More particularly, *Fig. 10* represents the critical shear rate as a function of the blend composition for the three systems. It is evident that a primary role is played by the component present with a high concentration and thus for φ = 25 percent the $\dot{\gamma}_c$ values are mostly the same as those of the pure LL samples while for φ = 75 percent, the $\dot{\gamma}_c$ are very similar to the value corresponding to the pure LD. *Figure 11* represents then the critical shear stress as a function of composition. In such a case, observations similar to the ones above can be made although the differences are much smaller. It is, incidentally, well known that τ_c does not depend strongly on the type of polymer.

Finally, regarding the non-isothermal elongational tests, *Fig. 12* shows the melt strength values, *MS*, as a function of the flow rate in the capillary, for all systems. When the low density sample (which has a *MS* value in all cases much higher than those of the pure LL samples) is mixed with LL0.5 or LL1, the blends exhibit a large increase in melt strength. At some composition, *MS* for the blends is even larger than for pure polymers. The same is not true for the LL4/LD, in which blends have intermediate *MS* values. The above data are replotted in *Fig. 13* as melt strength *vs.* the composition at a constant flow rate.

Figure 14 represents the breaking stretching ratio, *BSR*, data as a function of the flow rate, again for all systems. As is already well known, one observes that the LL samples have a much higher extensibility than LD. An antagonistic

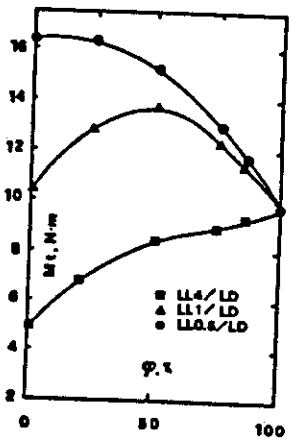

Fig. 8. Torque values as a function of the composition.

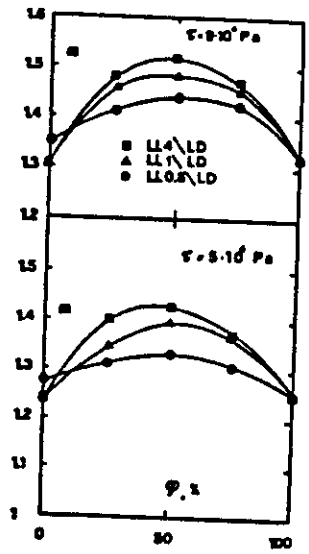

Fig. 9. Extrudate-swell as a function of the composition at two fixed constant stress.

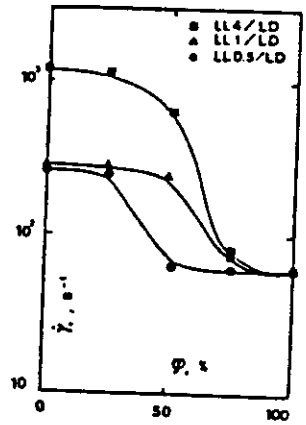

Fig. 10. Critical shear rate as a function of the composition.

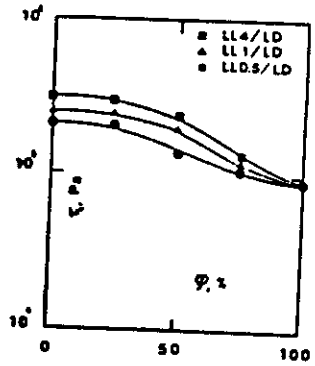

Fig. 11. Critical shear stress as a function of the composition.

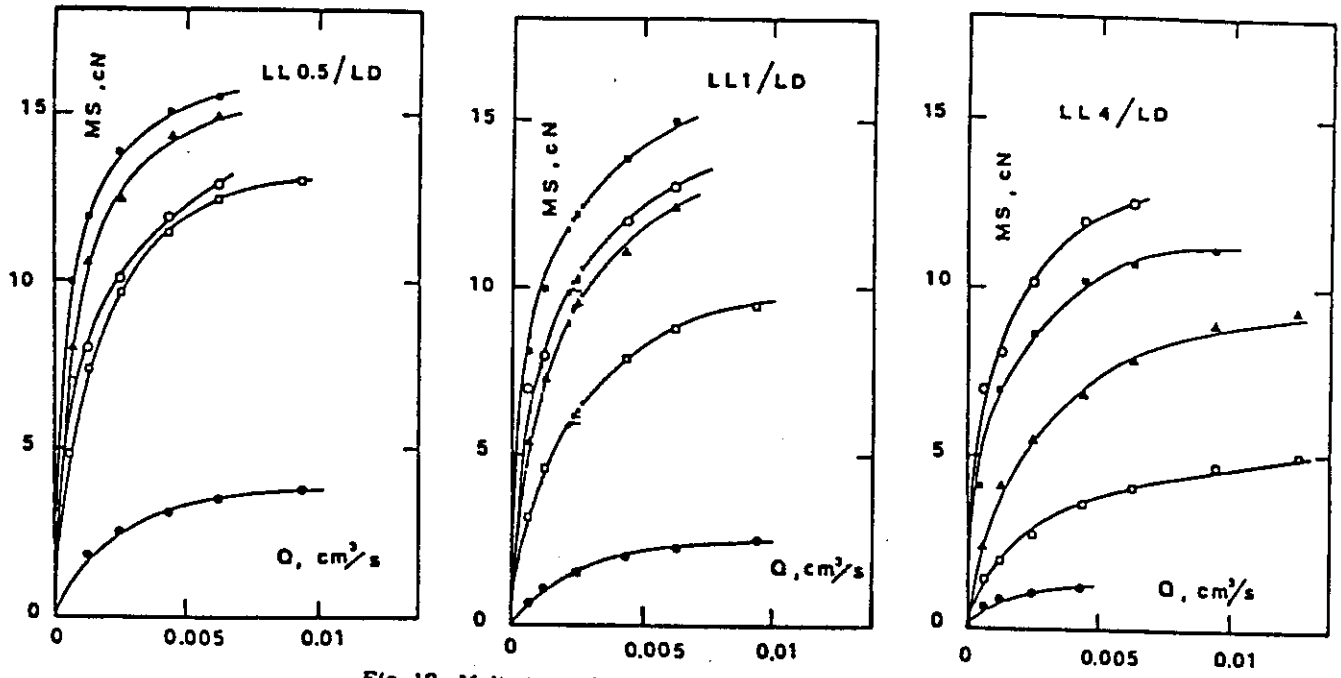

Fig. 12. Melt strength (MS) as a function of the flow rate.

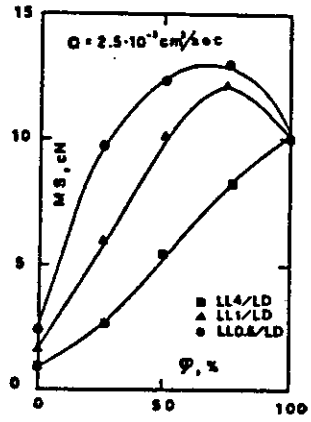

Fig. 13. Melt strength as a function of the composition at given flow rate.

effect is now present for the blends containing LL0.5 and LL1, and the minimum in the *BSR* can be better seen in *Fig. 15*. As expected, the minimum appears at the composition where a maximum was present in the *MS-φ* plot. For the LL4/LD system although an evident decrease of the *BSR* with the LD content is present, the values are always larger than those corresponding to the pure low density polyethylene sample.

CONCLUSION

From the full body of rheological data presented, one may conclude that the blend LL4/LD containing about 25 percent of linear low density polyethylene is the most interesting in view of the substituting of the low density poly-

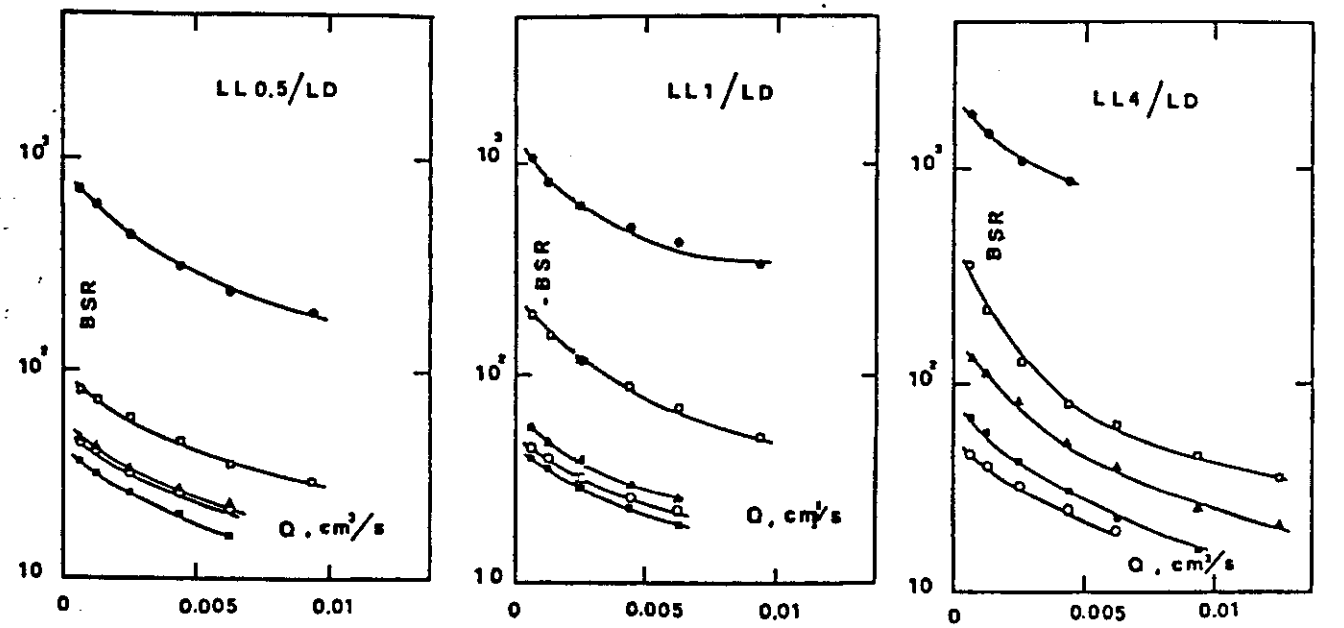

Fig. 14. Breaking stretching ratio (BSR) as a function of the flow rate.

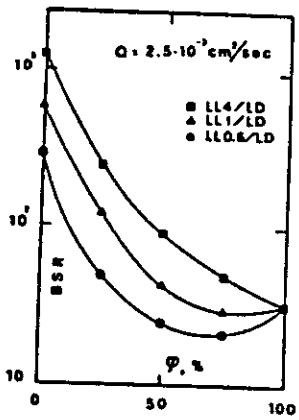

Fig. 15. Breaking stretching ratio as a function of the composition at given flow rate.

ethylene in the production of films by film blowing. It shows a similar shear viscosity, at the shear rates usually found in production, a melt strength only slightly lower, and a breaking stretching ratio larger than that of the LD sample. This should allow the production of thinner films without a too much larger consumption increase, somehow expected also because of the necessary rise of die temperature. Some preliminary results indicate that these blends also present interesting mechanical properties (17, 22).

ACKNOWLEDGMENT

This work has been carried out with the financial support of "Progetto Finalizzato del C.N.R. Chimica Fine e Secondaria."

Thanks are due to "Istituto per la Chimica e la Tecnologia dei Materiali Polimerici" for allowing use of the Rheotron and of the Rheoscope 1000 and to CEAST for allowing use of the tensile module.

REFERENCES

1. J. A. Manson and L. H. Sperling, "Polymer Blends and Composites," Plenum Press, New York (1976).
2. D. R. Paul and S. Newmann, Eds., "Polymer Blends," Academic Press, New York (1978).
3. O. Olabisi, L. M. Robeson, and M. Shaw, "Polymer-Polymer Miscibility," Academic Press, New York (1979).
4. A. P. Plochocki, *J. Appl. Polym. Sci.*, 16, 987 (1972).
5. A. P. Plochocki, *Trans. Soc. Rheol.*, 20, 287 (1973).
6. L. A. Utracki and M. R. Kamal, *Polym. Eng. Sci.*, 22, 96 (1982).
7. F. P. La Mantia, D. Acierno, and D. Curto, *Rheol. Acta*, 21, 452 (1982).
8. L. A. Utracki, Proceedings of IUPAC, Amherst, Mass., July 12–17, 1982.
9. L. A. Utracki, *Polym. Eng. Sci.*, 23, 602 (1983).
10. M. M. Dumoulin, C. Farha, and L. A. Utracki, *Polym. Eng. Sci.*, 24, 1319 (1984).
11. A. P. Plochocki, *Polym. Eng. Sci.*, 22, 1153 (1982).
12. L. A. Utracki and M. M. Dumolin, *SPE ANTEC Tech. Pap.*, 28, 51 (1982).
13. D. Curto, F. P. La Mantia, and D. Acierno, *Rheol. Acta*, 22, 197 (1983).
14. F. P. La Mantia, D. Curto, and D. Acierno, *Acta Polym.*, 35, 71 (1984).
15. D. Acierno, F. P. La Mantia, and D. Curto, *Polym. Bull.*, 11, 223 (1984).
16. A. Valenza, F. P. La Mantia, and D. Acierno, *Europ. Polym. J.*, 20, 727 (1984).
17. D. Acierno, D. Curto, F. P. La Mantia, A. Valenza, and A. Brancaccio, Proceedings of "Future Trends in Polymer Science and Technology, Polymer Commodities or Specialities" Capri, Italy, October 8–12, 1984.
18. F. P. La Mantia and D. Acierno, *Polym. Eng. Sci.*, to be published.
19. R. A. Mendelson and F. L. Finger, *J. Appl. Polym. Sci.*, 17, 797 (1973).
20. E. B. Bagley, *J. Appl. Phis.*, 28, 624 (1957).
21. B. Rabinowitch, *J. Phys. Chem.*, A145, 1 (1929).
22. F. P. La Mantia and D. Acierno, *Europ. Polym. J.*, in press.

NOMENCLATURE

e	= Bagley's correction factor.
v_m	= Specific volume at the extrusion temperature.
B	= Swelling ratio.
BSR	= Breaking stretching ratio.
D	= Capillary diameter.
D'	= Extrudate diameter.
L	= Capillary length.
M_n	= Average number molecular weight.
M_w	= Average weight molecular weight.
MFI	= Melt flow index.
MS	= Melt strength.
Q	= Flow rate.
$\dot{\gamma}$	= True shear rate.
$\dot{\gamma}_{app}$	= Apparent shear rate.
$\dot{\gamma}_c$	= Critical shear rate.
η	= Viscosity.
ρ	= Density at room temperature.
τ	= Shear stress.
τ_c	= Critical shear stress.
φ	= LDPE content.

DISCUSSION: D. CURTO

L. A. Utracki: Could you please explain what are the *BSR* and *MS* and how are they measured? Are they related to each other?

D. Curto: The *BSR* is a ratio of two velocities, the highest stretching velocity at break divided by the melt velocity in the die. The *MS* is given by the force at break. The instrument gives us directly both the velocity and the force at break. We note that as *BSR* increases *MS* decreases. Both are very important processing parameters.

D. Froelich: Apparently you measured the Newtonian viscosity at low rate of shear. Did you try to plot these as a function of composition to see what type of dependence they follow?

D. Curto: In *Figs. 5* to *7* the curves relative to $\tau = 3 \cdot 10^2$ Pa correspond to the Newtonian viscosity as a function of the composition. In all cases neither a linear nor a logarithmic rule is obeyed.

A New Method of Preparation of a Rubber-Modified Polyamide Directly During Caprolactam Polymerization

S. Cimmino, L. D'Orazio, R. Greco, G. Maglio, M. Malinconico, C. Mancarella, E. Martuscelli, P. Musto, R. Palumbo and G. Ragosta

Istituto di Ricerche su Tecnologia
dei Polimeri e Reologia, C.N.R.
Arco Felice, Naples, Italy

A New Method of Preparation of a Rubber-Modified Polyamide Directly During Caprolactam Polymerization

S. CIMMINO, L. D'ORAZIO, R. GRECO, G. MAGLIO, M. MALINCONICO, C. MANCARELLA E. MARTUSCELLI*, P. MUSTO, R. PALUMBO, *and* G. RAGOSTA

Istituto di Ricerche su Tecnologia dei Polimeri e Reologia, C.N.R., Arco Felice, Naples, Italy.

A new method to obtain a rubber-modified polyamide 6 (PA6) directly during the polymerization of the caprolactam (CL) is described. Binary and ternary blends containing ethylene-propylene random copolymers (EPM) and/or a functionalized EPM rubber (EPM g SA) were prepared and their morphology as well as their mechanical properties were investigated as function of composition and reaction conditions. It was found that the morphology of the blends is strongly dependent on the method of preparation. More complex structures are observed in blends obtained with the "Solution" preparation. For a better resolution of the morphology, the smooth ultramicrotomed surfaces were exposed to boiling xylene before SEM (scanning electron microscopy) examination. The rubbery phases are selectively dissolved whereas the PA6 matrix is left. The tensile mechanical properties and the Izod impact behavior are related to the mode and state of dispersion of the rubbery components. The impact properties of ternary PA6/EPM/EPM g SA (80/18/2) and (80/15/5) blends, prepared during the CL polymerization are comparable to those of similar blends obtained by usual melt mixing procedures.

INTRODUCTION

In a previous paper we described the conditions to functionalize an amorphous random ethylene-propylene rubber copolymer (EPM) by solution grafting of maleic anhydride molecules (1, 2). The reaction was promoted by radical initiators. The resulting modified rubber, EPM g succinic acid (EPM g SA), together with EPM, were used to prepare binary and ternary blends with polyamide 6 (PA6), by melt mixing, in order to obtain a rubber modified PA6 with better impact properties at temperatures below room temperature (1, 2). It was found that binary PA6/EPM g SA and ternary PA6/EPM/EPM g SA blends with compositions 80/20 and 80/10/10, respectively, show a significant improvement in impact strength. Such a result was interpreted by assuming that during melt blending an (EPM g SA) g PA6 graft copolymer is formed, acting as an interfacial agent, and thus influencing the overall morphology of the system (1, 2).

More recently the influence of different melt mixing procedures on morphology and on mechanical properties of the same type of rubber modified blends was investigated.

It was found that the overall morphology may be drastically changed and a finer dispersion of the rubber components may be reached by using more suitable mixing procedures. With this new preparation method, rubber-modified PA6 with still better impact properties may be obtained (3).

In the present paper we report on the results of an investigation concerning a new method to obtain a rubber modified PA6 directly during the caprolactam polymerization.

Binary and ternary blends containing EPM and EPM g SA rubbers were prepared and their properties and morphology studied and compared with those of blends prepared by melt mixing procedures.

EXPERIMENTAL

Materials

As the rubbery component, an amorphous Dutral Co/054, ethylene-propylene copolymer (EPM) having 60 percent by mole of C_2, kindly supplied by Montedison, was used. A modified EPM was

Caprolactam (CL) and aminocaproic acid (ACA) were FLUKA purum products used without further purification. Xylene, Carlo Erba RPE grade, was passed over neutral alumina and collected under nitrogen before use.

Preparation of a Typical Ternary Blend

The blends were prepared according to two slightly different procedures and coded as "S" and "B" types. "S" blends contain only 20 percent whereas "B" ones contain 20 percent by weight of initial total rubber (EPM and EPM-g-SA). The subscript of the complete codes reported in all the tables and figures stands for the EPM g SA weight percentage.

"S" coded blends

In a glass vial, equipped with a side arm, 8.0 g of EPM and 2.0 g of EPM-g succinic acid (3 percent by weight of succinic acid) were dissolved in 170 cc of anhydrous and repeatedly degassed xylene by refluxing under nitrogen atmosphere. After dissolution, 90.0 g of CL and 2.0 of ACA were added without occurrence of a clear phase separation. By raising the temperature to 200°C, the xylene was slowly distilled through the side arm in a graduated recovery flask. The last traces of xylene were removed at 260°C and 600 torr. More ACA (2.5 g) was added and the polymerization was carried out for 4 hrs at 260 to 270°C under a slow stream of nitrogen and vigorous mechanical stirring.

The crude reaction mixture, 103 g, was finely ground, extracted in a soxhlet apparatus for 24 hrs with boiling methanol and dried under high vacuum at 130°C for 24 hrs (18.2 percent MeOH extractable evaluated only on polyamide fraction). A polyamide sample recovered by formic acid extraction had η_{inh} = 1.24 dl/g (in cresol; T = 25°C; c = 0.5 g/dl) and M_n = 2.10 × 10^4 (4).

"B" coded blends

The synthetic procedure for a "B" coded blend is substantially similar to that previously described for the S blend, but no xylene was used to "homogenize" the components, and therefore the distillation step was unnecessary, and the ACA was added all at once together with the CL. The yield of reaction, MeOH extractable products and M_n are essentially the same as above.

Specimen Preparation and Conditioning

The material obtained by synthesis was compression molded in a common heated press at a temperature of 200°C and a pressure of 9 10 kg/cm² into sheets of two different thicknesses (1 and 4 mm). From 1 mm thick sheets dumbell shaped specimens for mechanical tensile tests were cut by a suitable hollow punch.

From 4 mm thick sheets, parallelepipedal specimens (60 by 13 by 4 mm) for Izod impact tests were obtained by means of a milling machine. On such specimens a 2 mm deep notch with a curvature

of samples were conditioned in water at 90°C in order to obtain in any case the same amount of absorbed water (about 3 percent by weight). The procedure is reported elsewhere (2).

1.4 Techniques

Mechanical Tensile Tests

Stress strain curves, for all the blends reported in *Table 1*, were carried out by an Instron machine (Model 1122) at room temperature and at a crosshead speed of 20 mm/min.

Morphological Analysis

Before electron microscopy studies, samples of binary and ternary blends were faced in a ultramicrotome (LKB Ultrotome III) at room temperature. The smooth surfaces were coated with gold/palladium and then examined by using a Philips 501 scanning electron microscope.

For a better resolution of the morphology an etching technique based on the preferential rubber dissolution by means of xylene was developed. Microtomed surfaces of binary and ternary blends were exposed to xylene vapors or directly dipped in boiling xylene and subsequently prepared for SEM examination. It was observed that the rubbery phase is readily dissolved by xylene while the PA6 remained unaffected.

Fractography

A morphological analysis of the Izod fracture surfaces as function of test temperature was performed by means of a Phillips 501 scanning electron microscope, after coating the broken surfaces with Au/Pd.

Impact Strength Measurements

Izod impact testing was made by using a fracture pendulum (Ceast Autographic Pendulum) in the temperature range from −25°C up to room temperature.

RESULTS AND DISCUSSION

Synthesis of Rubber-Modified Polyamide 6

The synthesis of the succinic acid modified rubber (EPM g SA) has been previously reported (1, 2). In this work we used an EPM g SA bearing 3 percent by weight of succinic acid. The hydrolytic

Table 1. Preparation of rubber-toughened Polyamide 6 by bulk and solution methods.

Blend code	Feed Composition by weight				Preparative method
	CL	ACA	EPM	EPM g SA	
P	80.0	2.0	0	0	bulk
P_{10}	80.0	2.0 (1.6 h)	10	0	solution
P_8	80.0	2.0 (1.6 h)	8	2	solution
P_{10}	80.0	2.0 (1.6 h)	0	10	solution
P_{20}	70.0	4.0	20	0	bulk
P_8	70.0	4.0	16	4	bulk
P_{16}	70.0	4.0	16	4	bulk

synthesis of polyamide (PA6) has been recently reviewed by Sebenda (5); and may be summarized by the following equilibria: [illegible] CL

EPM-g-SA mixture no phase separation was apparent in the ternary CL/EPM/EPM g SA, a fine and stable suspension of rubber in CL was observed, while in the binary CL/EPM mixture a coarse phase separation was found to occur. These findings are likely to be related to some emulsifying effect of compound I (see *Eq 4*).

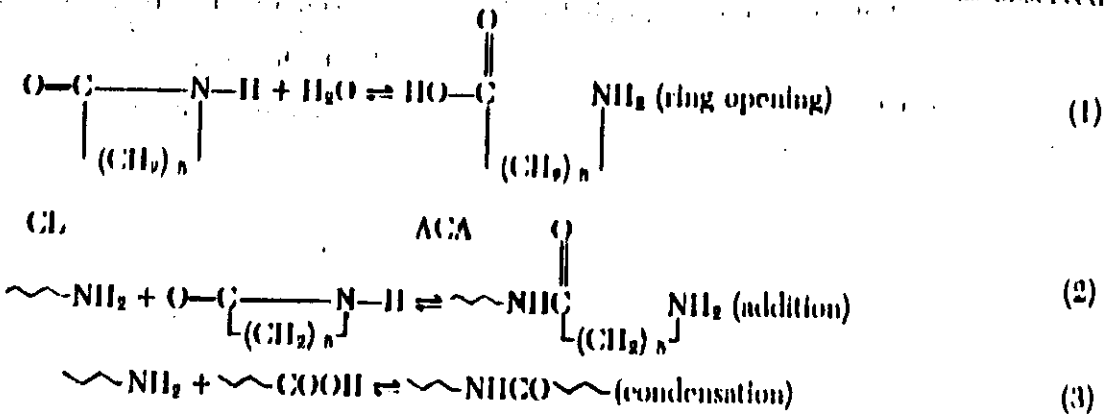

Instead of using water, we added ACA directly as initiator. It is likely that in the early stage of polymerization EPM-g-SA may be at least partially involved in the following side equilibrium:

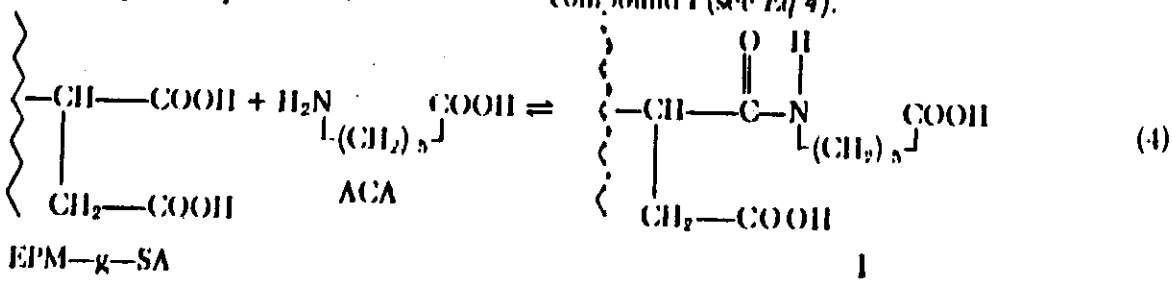

As matter of fact, IR analysis of the rubbery component recovered from the reaction mixture in the early stages of the polymerization shows the presence of both amide and acid –C = O stretching absorptions at 1705, 1645 and 1535 cm^{-1} in agreement with structure I.

Subsequently intermediate I will be probably involved in a polycondensation equilibrium with PA6 growing chains giving rise to the formation of a (EPM g SA) g PA6 graft copolymer.

Appropriate modifications of the standard conditions used to homopolymerize PA6 were tested in the preparation of blends of PA6 and EPM and/or EPM-g-SA in order to ensure both a high polymerization degree and good dispersion of the rubbery component. In *Table I* are summarized blend codes, compositions and preparative methods of investigated binary and ternary blends. For sake of comparison we have also prepared a PA6 homopolymer sample under the same experimental conditions.

Because EPM and EPM g SA are both immiscible with CL, in the earlier experiments concerning the preparation of blends with 10 percent by weight of total rubber, the "homogenization" of the reaction mixture was accomplished by first dissolving EPM and/or EPM g SA in xylene at 130°C and by subsequently adding CL and ACA ("S" coded series). The temperature was left to rise to 200 to 210°C while xylene distilled off.

At this stage, when CL polymerization is not yet started, we have found that the presence of EPM

So all amounts of water, deriving from stage 1, were found to distill together with xylene. This and the consumption of ACA via equilibrium 4 causes a lowering of initiator concentration which was balanced by adding more ACA.

The CL polymerization was subsequently carried out at 260 to 270°C for 4 hrs under N_2 atmosphere and vigorous mechanical stirring. Absence of oxygen was necessary in order to avoid yellowing of the polymerization mixture.

Visual observations of the molten mixtures at the end of the polymerization indicated that the dispersion of the rubbery domains into the blend increases gradually with the amount of the added modified EPM.

As results on analogous blends prepared by melt mixing (1–3) showed that higher contents of total rubber were necessary to significantly improve the impact properties, we investigated the preparation of a new series of binary and ternary blends containing 20 percent rubber by a hydrolytic process. Furthermore, in order to bring experimental conditions closer to those used in the industrial process of the hydrolytic polymerization of CL, we have also investigated the preparation of the above blends by a bulk process ("B" coded blends).

Accordingly, all the starting materials were mixed together, in absence of xylene, and CL polymerization was performed as described for the "S" series (no further addition of ACA is needed during this process).

dispersion of components.

It is interesting to note that under our experimental conditions and using a mechanical stirrer in a cylindrical glass vial, blends with a total rubber content of 20 percent in which the ratio EPM-g-SA/total rubber exceeds 0.25 were too viscous to be efficiently stirred. Therefore only ternary blends containing 2 and 5 percent modified rubber could be prepared. The yields of the crude polymerization products are almost quantitative. A methanol soluble fraction was found, as generally occurs in PA6 samples prepared by ring opening of CL (4). This fraction is mainly formed by equilibrium monomer and lower cyclic oligomers. In *Table 2* some characterization data of the blends are reported. Formic acid extractions of the methanol insoluble products may be used to obtain pure PA6 from the blends as PA6 is soluble while EPM separates as a supernatant solid phase. This technique was found suitable only for S_0, S_2, B_0, and B_2 blends, where little or no (EPM-g-SA)-g-PA6 graft copolymer is present. In B_5 the larger amount of (EPM-g-SA)-g-PA6 graft copolymer, acting as emulsifier, causes such a delay of the phase separation phenomenon that clear solutions cannot be obtained even after months. On the other hand, a clear solution is obtained in the case of S_{10} blend indicating that all the PA6/EPM graft copolymer is solubilized in the formic acid or is at least very finely dispersed.

These results, which may be regarded as Molau tests (6), clearly show the emulsifying effect of the (EPM-g-SA)-g-PA6 copolymer. The molecular mass of the polyamide samples recovered from S_0, S_2, B_0, and B_2 blends are satisfactory and practically identical to that of a pure PA6 sample prepared in a test-experiment (see *Table 1*).

Specimen Characterization

Tensile Mechanical Properties

Stress-strain curves at room temperature for PA6 homopolymer and for all the binary and ternary blends investigated are reported in *Fig. 1*. The behavior goes from a very ductile fracture of pure PA6 to a less ductile one, depending on the blend type and composition. The Young modulus (*E*) of blends is lower than that of plain PA6 and in all cases decreases with an increase of the overall rubber content. This behavior is probably due to the decrease of the overall crystallinity content of the material.

The ultimate properties and particularly the elongation at break (ϵ_b) seem to be more interesting as sources of structural information. Such a parameter shows very high values (400 percent of total deformation) for PA6 (curve P), whose specimens appear to be still transparent after stretching. The ϵ_b of S_0 and S_2 samples decrease to about 140 percent and their specimens show a stress whitening phenomenon probably due to diffuse craze formation around the rubber particles during elongation. Such an effect is higher in the case of S_{10} blend where the (EPM-g-SA)-g-PA6 graft copolymer cannot act as

blends.

Blend code	MeOH soluble, percent	Composition (PA6/EPM/EPM-g-SA) Initial	Final	M_n*
P	20.3	100/0/0	100/0/0	22.100
S_0	15.2	90/10/0	88/12/0	18.400
S_2	16.2	90/8/2	87.5/10/2.5	21.600
S_{10}	15.2	90/0/10	88/0/12	—
B_0	22.0	80/20/0	74.4/25.6/0	21.000
B_2	24.7	80/18/2	74.4/23/2.6	19.500
B_5	21.0	80/15/5	74.7/19/6.3	—

* Number average molecular weight of PA6 recovered from the blend, determined according to Ref. 4.

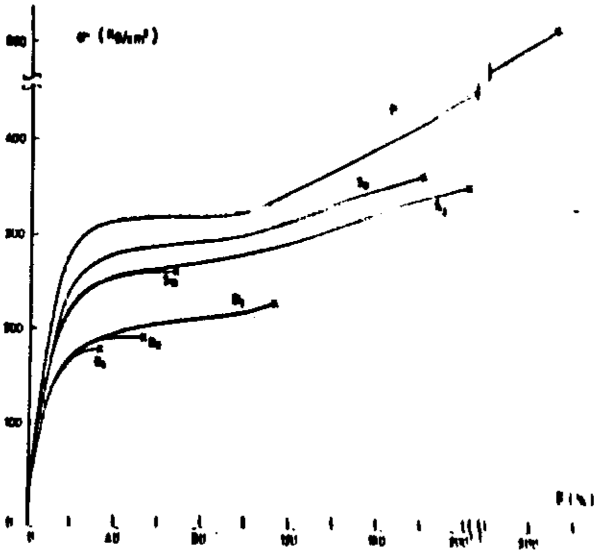

Fig. 1. Stress-strain curves for PA6, binary and ternary blends.

interfacial agent because no EPM rubber is present. The elongation at break of the S_{10} blend is lowered to about 65 percent. This low ϵ_b value is due to the influence of the high (EPM-g-SA)-g-PA6 content, which renders the system more strongly interconnected and therefore less able to undergo the cold-drawing process (see *Fig. 4e*).

For the *B* blends, containing 20 percent total rubber, the elongation at break values are 30 percent for B_5, 50 percent for B_0, and 110 percent for B_2. Moreover the B_2 specimens exhibit a slight stress whitening effect due to a multiple crazing mechanism acting in the material during its elongation. The craze formation produces an apparent volume increase of the blend and hence generates ϵ_b values higher than those corresponding to B_0 and B_5 samples, for which no stress whitening effect is observed.

The lower ϵ_b values of B_0 and B_5 depend on different reasons. For B_0 blends, the presence of very large EPM domains as observed in SEM micrographs (see *Fig. 5*), may hamper the cold drawing and cause the premature fracture of the specimen. The coarse dispersion of rubber particles can be related to the weak stirring power of the system during and at the end of polymerization. For B_5 blends the situation may be even worse because, as previously mentioned, the melt viscosity of blends increases with increasing EPM-g-SA content and therefore in this [illegible]

also present (see Fig. 7). Moreover at least part of the functionalized rubber is converted to (EPM g SA)-g-PA6, which acting as an interfacial agent between matrix and dispersed phase, renders the system locally more interconnected and hence less capable of cold-flow.

Numerical values of E, σ_b, and of the ultimate tensile strength (σ_R) are reported in *Table 3* as a function of the total rubber amount in the blends.

From these data it emerges that blends have values of σ_R lower than that of PA6. This decrease seems to be larger in the case of blends with a higher EPM-g-SA content (S_{10} and B_{10}).

Morphology of Microtomed Blend Surfaces

Scanning electron microscopy in most cases is a powerful technique for direct visualization of distinct phases in heterogeneous blends, but sometimes, when the contrast is low, it is unable to provide detailed information about the composition and microphase structure of the system.

A useful technique in such cases is to selectively remove one phase from the blend surface by etching or by dissolution and subsequently examining the resultant topography. Such an approach was followed in the present study.

Samples of binary and ternary blends were faced in an ultramicrotome at room temperature; subsequently the smooth surfaces were exposed to boiling xylene vapors or immersed in boiling xylene before being prepared for SEM examination. The rubbery phase is selectively dissolved by xylene whereas the PA6 matrix remained unaffected.

Morphology of S-coded blends

Figure 2a shows SEM micrograph of the untreated smooth surface of the S_0 sample. As can be seen, the EPM segregates from the PA6 matrix in spherically shaped domains regularly distributed throughout the whole surface. Exposure to boiling xylene vapors for 30 min produces holes corresponding to the dissolution of the EPM inclusions and evidences the wide size distribution of such domains, ranging from 5 μ to about 20 μ (*Fig. 2b*).

The complete dissolution of EPM seems to suggest that there is no adhesion at the interface with the PA6 matrix. This conclusion is strongly supported by the fractography analysis as reported elsewhere in this paper. In the case of S_{10} blends, protrusions emerging from the dispersed domains

Table 3. Tensile modulus, strength, and elongation at break as a function of compositions

Code	$E \times 10^{-3}$ (Kg/cm^2)	σ_b (Kg/cm^2)	ε_b (percent)
P	3.0 ± 0.1	810 ± 90	300 ± 30
S_{10}	2.7 ± 0.1	800 ± 90	400 ± 20
B_{10}	2.2 ± 0.1	720 ± 40	60 ± 15
S_5	2.9 ± 0.1	900 ± 90	300 ± 30
B_5	2.4 ± 0.2	720 ± 20	110 ± 40
B_2	2.6 ± 0.1	800 ± 30	90 ± 10
B_1	2.7 ± 0.1	800 ± 30	90 ± 10

are clearly visible on the smooth surface (see *Fig. 3a*).

The etching of the surface with boiling xylene vapors is able to dissolve only part of the material contained in the dispersed domains, leaving the protrusion structures practically unchanged and isolated from the rest of the material (see *Fig. 3b* and *3c*). Moreover, such structures are connected to the underlying matrix. Such observations strongly indicate that in S_2 blends the dispersed domains are of a multiphase type, i.e., they contain a rubbery phase that is permeated by irregular polyamide structures protruding from the matrix and strongly bonded to it.

The presence of a certain amount of (EPM-g-SA)-g-PA6 graft copolymer may contribute, together with the shear stresses induced by the stirring system, to the formation of such a complicated overall morphology.

Smooth surfaces of the S_{10} binary blends show the presence of dispersed domains randomly distributed throughout the whole sample (see *Fig. 4a*). It is to be emphasized that the relative area occupied by such domains seems to be lower than the relative volume of the initially added EPM g SA.

As shown in *Fig. 4b* boiling xylene vapors are able

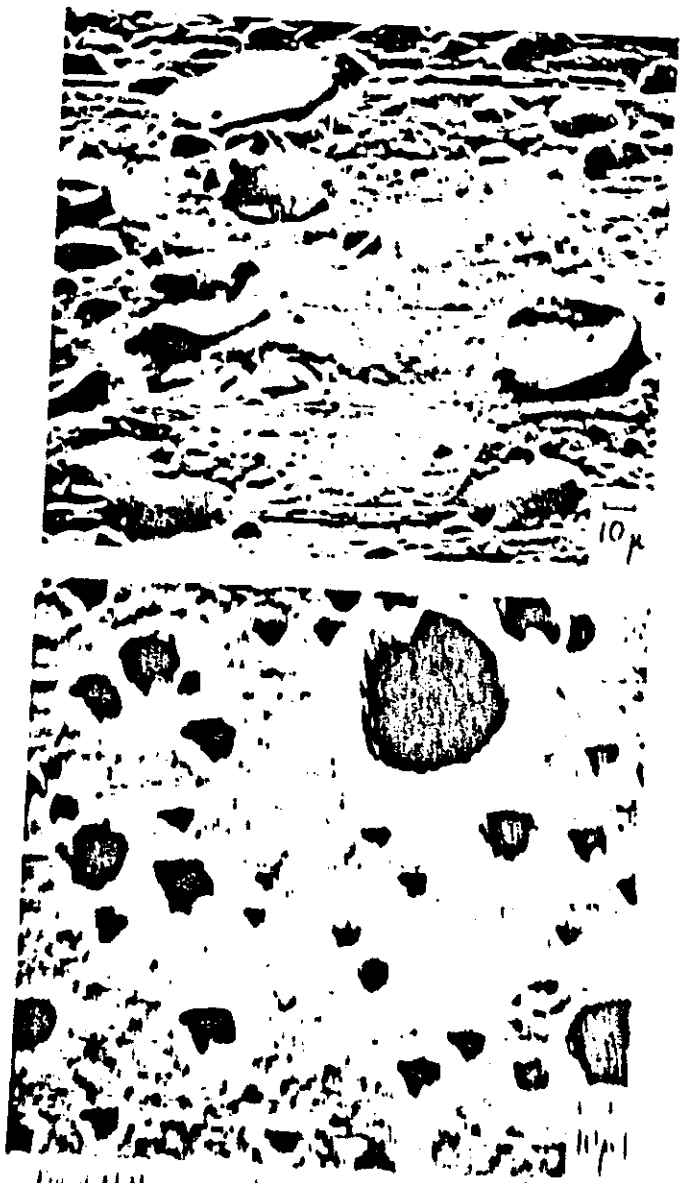

Fig. 2. SEM micrographs of smoothed surfaces of

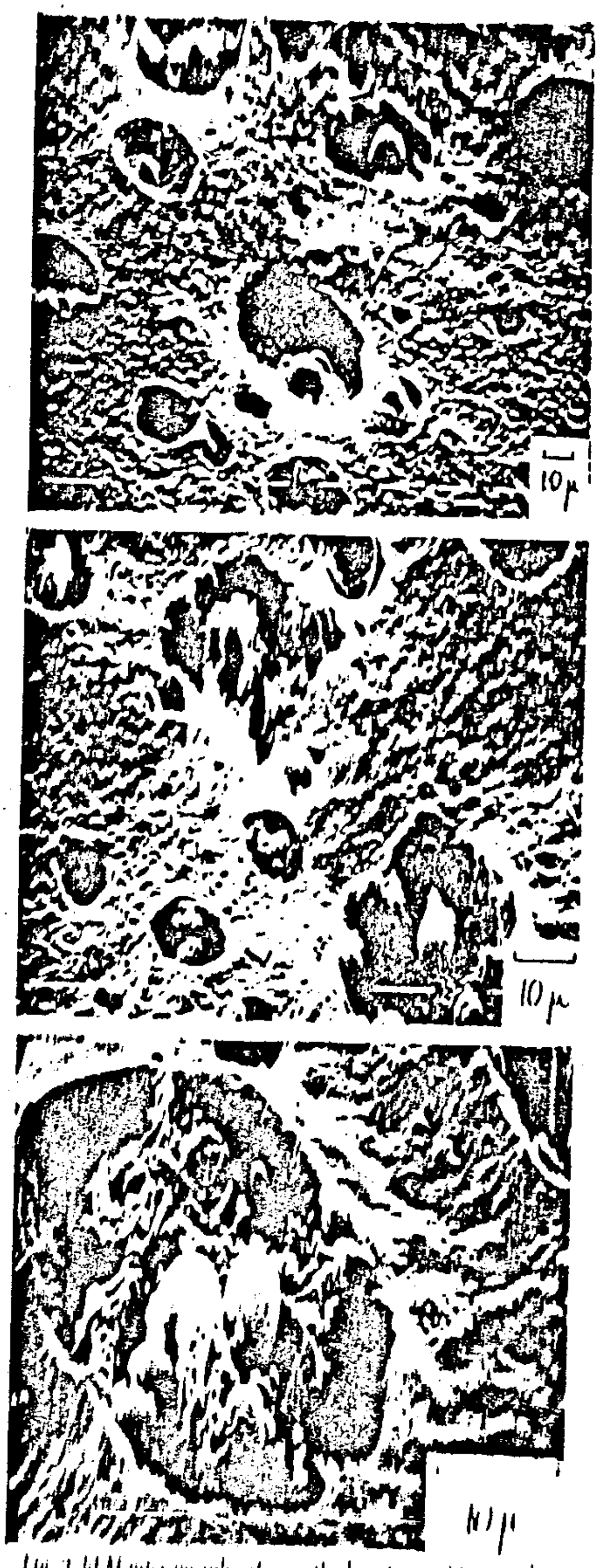

Fig. 3 SEM micrographs of smoothed surfaces of [illegible] sample
a) before etching (1000×)
b) after etching (1000×)
c) after etching (2500×)

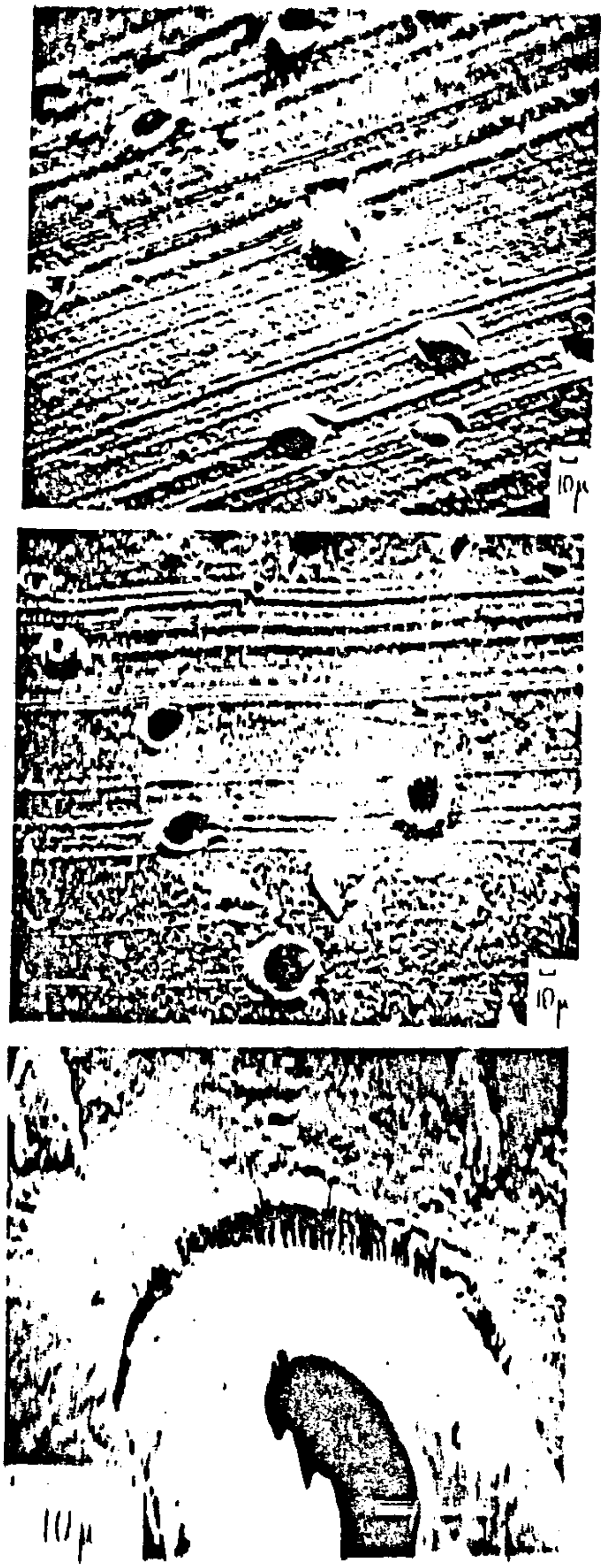

Fig. 4 SEM micrographs of smoothed surfaces 5% sample
a) before etching (1000×)
b) after etching (1000×)
c) after etching (2500×)

be dissolved completely, only the central region of such domains. Fibrils connecting the PSO matrix with the undissolved adjacent regions of the dispersed domains are clearly evidenced by the etching technique (see Fig. 3c).

The above observations may be accounted for by assuming that during the process of blend prepa- graft copolymer and that such copolymer at the end of the polymerization, because of a combined effect of the interfacial forces and of the shear stresses due to the mechanical stirring, organizes partially at least at the interface between the PSO and EPM-g-SA rubber, thus acting as a real interfacial agent. Consequently, the dispersed domains observed in

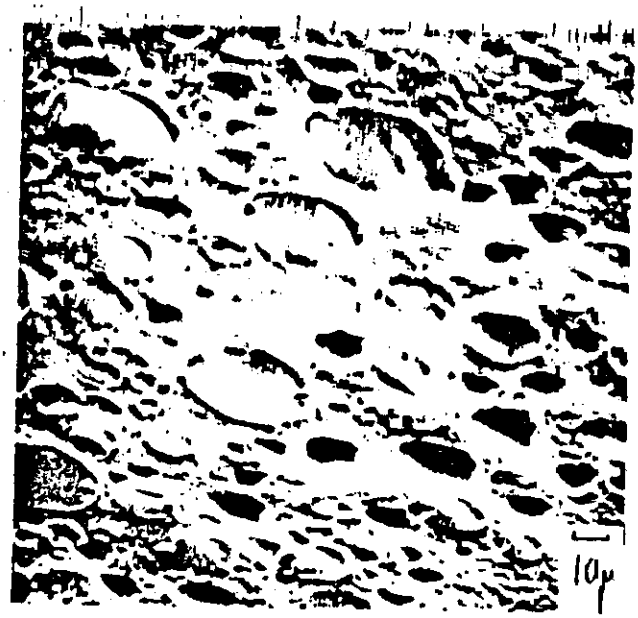

Fig. 5. SEM micrograph of smoothed surface of B_5 sample before etching (6400×)

Fig. 6. SEM micrograph of smoothed surface of B_5 sample
a) before etching (6400×)
b) after etching (6400×)

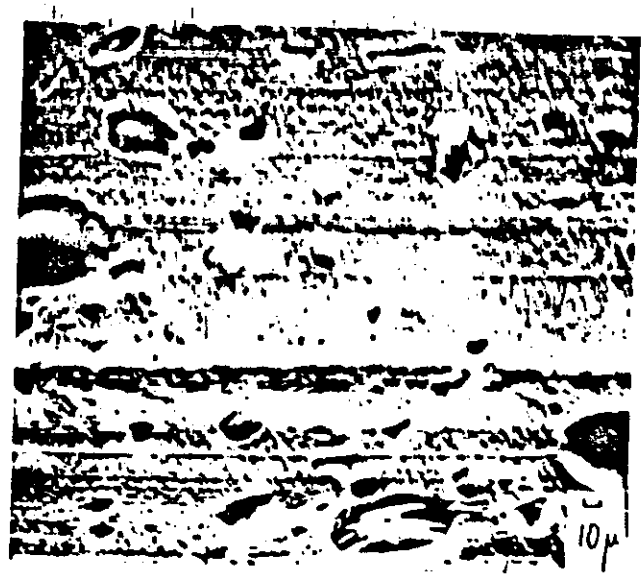

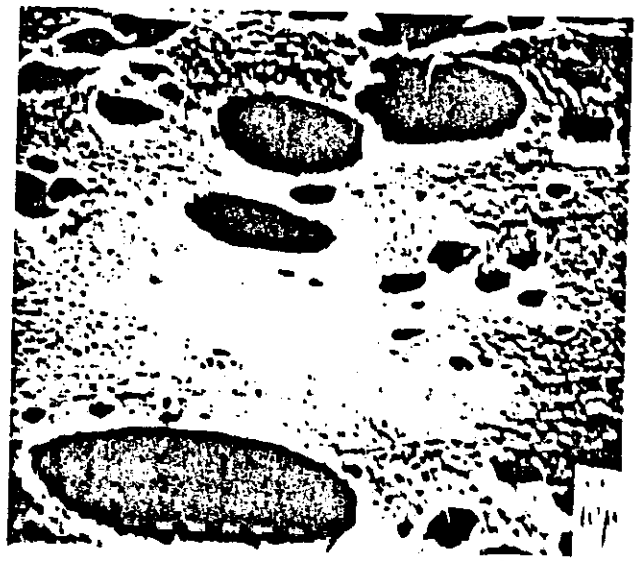

Fig. 7. SEM micrograph of smoothed surfaces of B_5 sample
a) before etching (3200×)
b) after etching (3200×)

B Coded Blends

In the case of blends with overall rubber content of 20 percent after the exposure of the smooth surfaces to boiling xylene vapours, the rubbery phase is not completely removed, and it was necessary to immerse the samples directly in boiling xylene. SEM studies performed on B_5 and B_6 specimens treated with boiling xylene for 15 min reveal well defined but irregular rubbery domains dispersed in the PA6 matrix with a wide size distribution (see Figs. 6 and 7). It is to be pointed out that for the ternary blends no protrusion structures are observed.

The boiling xylene in the case of B blends seems to be able to completely dissolve the rubbery domains, as shown by the smooth walls of the remaining cavities, contrary to what was observed for S type blends containing EPM g-SA. These morphological characteristics may suggest that the EPM g-SA/g-PA6 formed during the blend preparation process in bulk is quantitatively insufficient to act effectively as an interfacial agent and therefore the

polymer is finely dispersed in the PA6 matrix with no connection to the rubbery domains must be also taken into consideration. This phenomenon of "dissolution" could produce drastic modifications in some intrinsic matrix properties such as PA6 spherulite size and thus in the crack propagation mechanism.

Impact Properties

Fractographic Analysis

With the view of elucidating the influence of composition and test temperature on the mode and mechanism of fracture of "S" and "B" blends, a morphological analysis of fracture surfaces by means of SEM has been performed.

S-coded Blends

The fracture surfaces of PA6 homopolymer broken at −20°C (*Fig. 8a*) show no induction zone but only a fast crack propagation zone throughout the specimen. At −2.5°C, a limited induction zone begins to appear (see *Fig. 8b*) indicating that a transition from brittle to ductile behavior is occurring.

The S_{11} blend at −20°C (*Fig. 9a*) shows a fracture mechanism that is very similar to that of PA6 with a fast crack propagation zone extended to the whole sample but with a rougher surface indicating a slightly higher energy dissipation than in the case of PA6. Spherically shaped domains of EPM copolymer with a diameter ranging from 5 μm to 20 μm, randomly distributed throughout the whole surface are observed (see *Fig. 9b*).

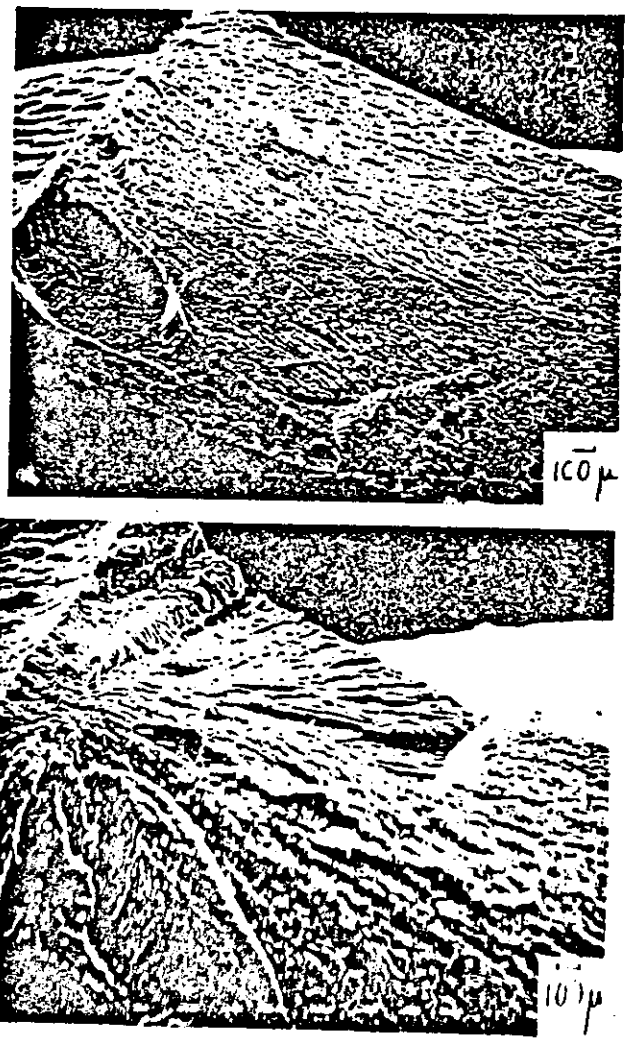

Fig. 8. SEM micrographs of fracture surfaces of PA6 sample at different test temperatures
a) + 20°C (40×)
b) − 2.5°C (40×)

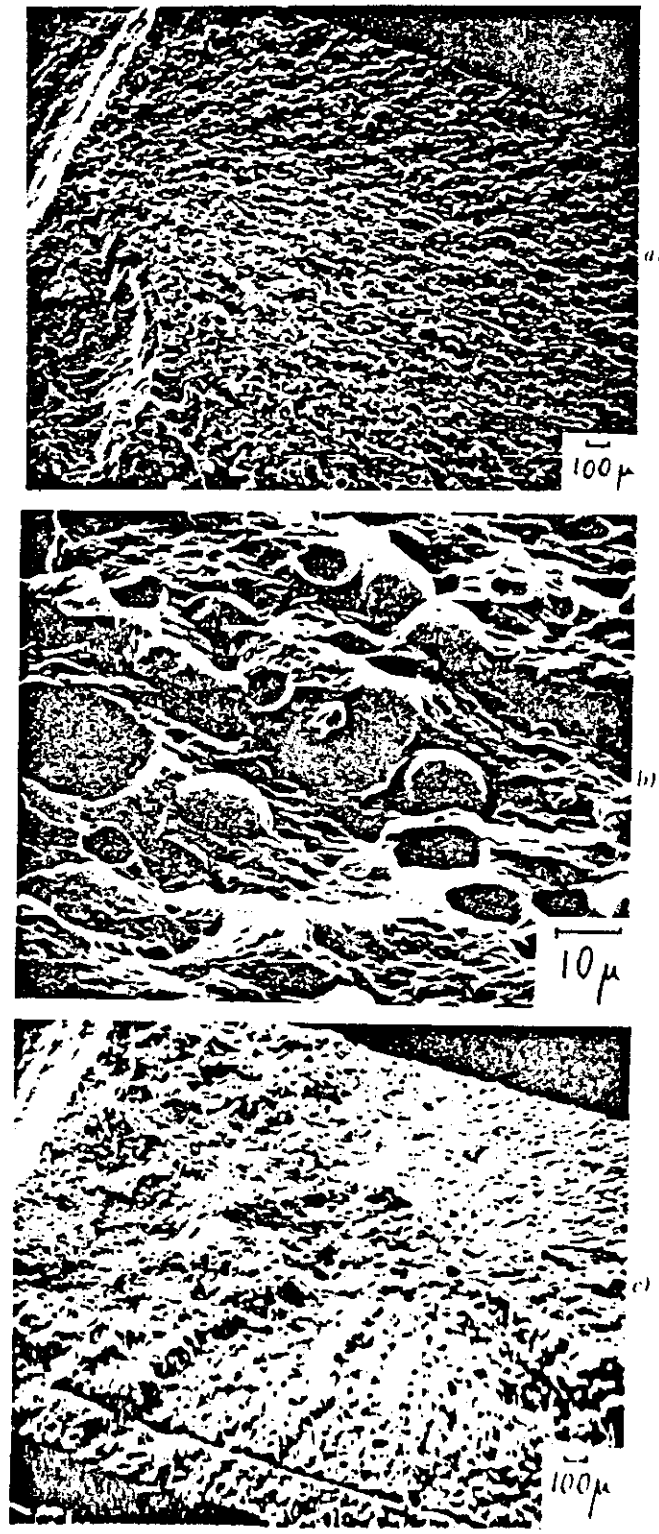

Fig. 9. SEM micrographs of S_{11} fracture surfaces at different test temperatures
a) −20°C (40×)
b) −20°C (1250×)
c) −11°C (40×)

Fig. 9 d) 11°C (1250×)

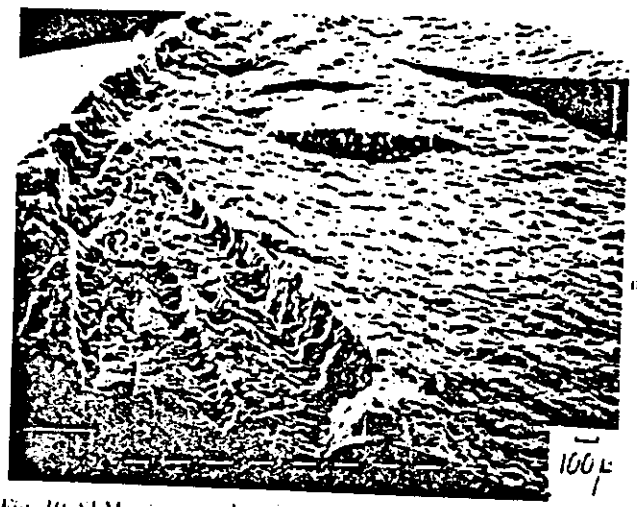

Fig. 10 SEM micrographs of S_2 fracture surfaces at different test temperatures
a) −20°C (40×)

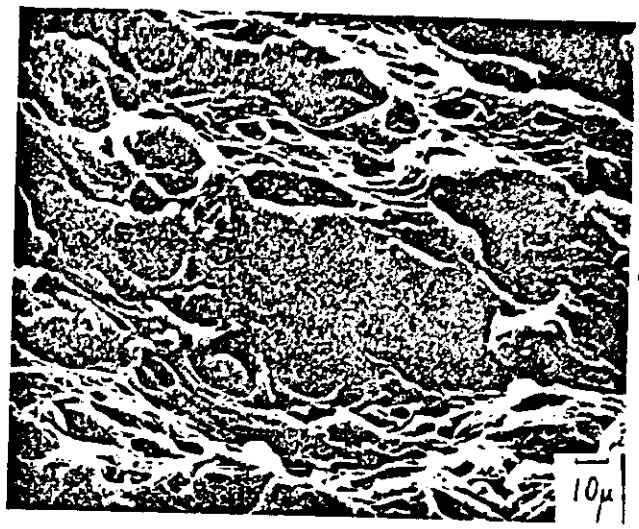

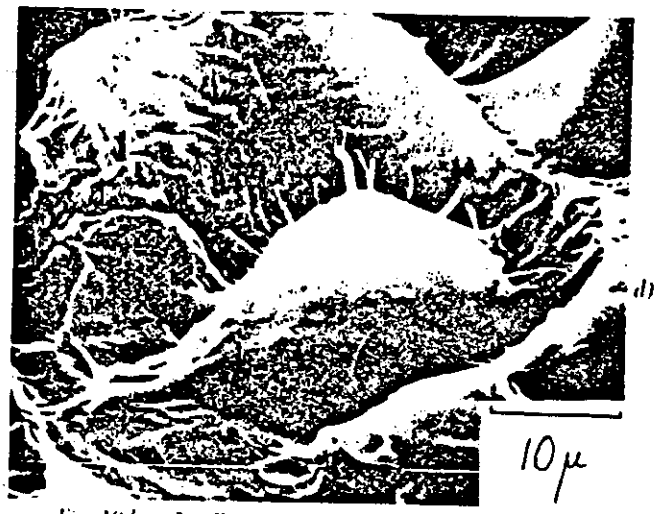

Fig. 10 b) −20°C (1250×)
c) −10°C induction region (640×)
d) +5°C (2500×).

No adhesion seems to exist between the dispersed particles and the PA6 matrix as evidenced by the very smooth walls of the cavities. The fracture process and, in turn, the morphology of the fractured surfaces of such a binary blend are drastically changed by increasing the test temperature.

SEM micrographs of broken surfaces of samples tested at 11°C show a distinct induction zone starting from the notch and covering a discrete area where the sample undergoes a plastic shear yielding mechanism (*Figs. 9c* and *9d*).

The remainder of the sample exhibits—as in the previous case—a sudden crack propagation. The area of the induction region increases with increasing test temperature.

At −20°C the S_2 ternary blend also fractures in a brittle manner. The fracture surface of such a mixture shows a macroscopic roughness (see *Fig. 10a*).

From a careful inspection of high-magnification SEM micrographs, there seems to be evidence of rubbery domains very well embedded into the PA6 matrix as suggested by the presence of regions with a very smooth surface structure (*Fig. 10b*). With increasing test temperature a distinct induction region of plastic deformation by a shear yielding mechanism appears (*Fig. 10c*). In this region irregularly shaped rubbery domains connected to the PA6 matrix by means of fibrils are observed (*Fig. 10d*). The above findings are further evidence that the formed (EPM-g-SA)-g-PA6 copolymer may act as an "interfacial agent" promoting the adhesion between the PA6 matrix and the rubbery dispersed phase.

Figure 11 shows SEM micrographs of fracture surfaces of S_{10} binary blend. At −20°C the macro-

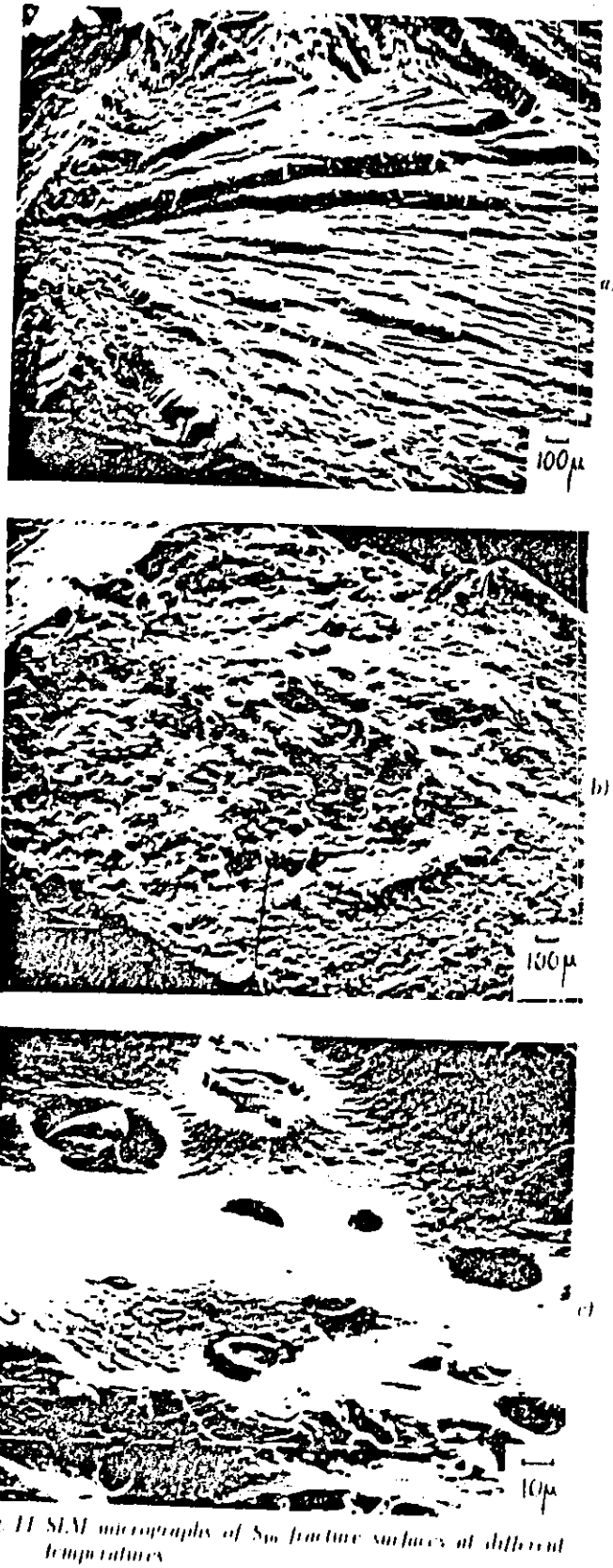

Fig. 11 SEM micrographs of S_0 fracture surfaces at different temperatures
a) −20°C (ductile)
b) 0°C (ductile)
c) 0°C (induction region (ductile))

Fig. 11 d) +9.5°C propagation region (5000×)

morphology of the broken surface is typical of a fast fracture exhibiting a rough elongated topography (*Fig. 11a*).

It is important to note that because of the high rate of crack propagation, no distinction between the phases can be observed at this temperature.

These morphological results are consistent with the glassy nature both of the matrix and copolymer at the temperature and rate of fracture.

With increasing temperature the samples undergo considerable plastic deformation and the fracture surface shows an induction region involving a larger area than in the case of the S_0 blend (*Fig. 11b*). In this region rubbery domains strongly adherent to the matrix are observed.

Such observations may have a more general significance; as they indicate that the morphology of a multiphase blend appears to be resolved into its structural elements, on Izod broken surfaces, only when the rate of crack propagation is low; in turn this depends upon testing temperature and type of fracture mechanism. It is interesting nevertheless that even in case of resolved morphology the elements may appear strongly deformed because of the fracture process and different morphological features may be seen in different regions of the broken samples surfaces according to the local rate of crack propagation. It may be concluded that the impact strength and mechanical properties of a multiphase blend should be more correctly correlated with morphological parameters that result from microtomed surfaces or thin sections etched by using suitable solvents, where the structural elements that emerge undergo only small deformations.

B Coded Blends

The morphological features observed on broken surfaces and the fracture mechanism exhibited by the B_0 binary blend are quite similar to those described by the S_0 mixture. However in the case of B_0 blends the average diameter of EPM domains is larger. This finding is partly due to the insufficient stirring of the mixture during the synthesis (compare *Fig. 12* with *Fig. 9b*).

Figure 13a shows SEM micrographs of B_0 fracture surfaces. At the lowest temperature ($T = -20°C$) the blend exhibits an irregular multicrack propagation process. It is possible to note, in fact, radial crack distributions around the largest rubbery domains. This can involve a certain amount of fracture energy dissipation even at such a temperature.

Fig. 12. SEM micrograph of B_5 fracture surface at −20 °C (40×)

Fig. 13. SEM micrographs of B_5 fracture surfaces at different test temperatures
a) −20 °C (40×)
b) −20 °C (640×)

Spherically shaped domains of the rubbery phase, randomly dispersed throughout the whole surface, with a wide size distribution can be observed (*Fig. 13b*). An increase of test temperature drastically changes the fracture mechanism. In fact, the whole sample undergoes a plastic deformation indicating

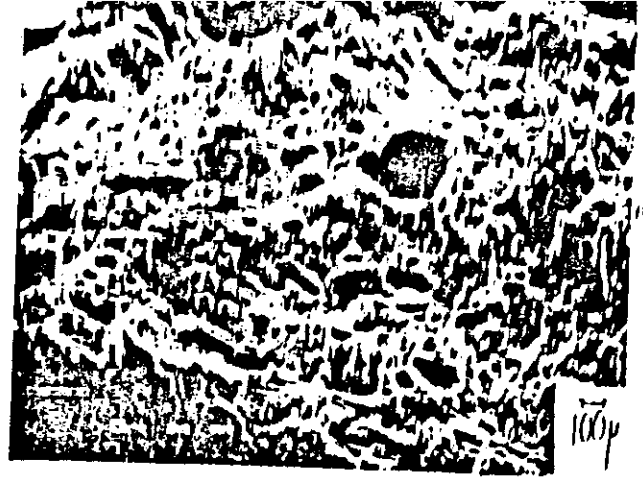

Fig. 13 c) +5 °C (40×)
d) +5 °C (640×).

a transition to a more ductile fracture behavior (*Fig. 13c*) consistent with a shear yielding fracture mechanism.

The fracture surface of the B_5 sample, broken at −20°C, exhibits a rough stepped topography typical of a fast fracture (see *Fig. 14a*). Because of the high rate of crack propagation, at this test temperature no distinction between the phases can be detected. A transition from a brittle to a ductile impact behavior by increasing temperature is produced.

SEM micrographs of broken surfaces show a clear limited induction region plastically deformed (*Fig. 14b*) with the material volume involved increasing with increasing test temperature. It is important to note the presence, in the slow crack propagation region, of well-defined rubbery domains, randomly distributed, showing a certain degree of adhesion to the PA6 matrix (*Fig. 14c*).

Izod Tests

The Izod impact strength values (R) for all the S and B coded blends are reported as a function of the testing temperature in *Figs. 15a* and *15b*, respectively. The PA6 homopolymer (curve P) exhibits very low R values at temperatures below −10°. In such regions the binary and ternary S blends show (see *Fig. 15*) only a slight increase of

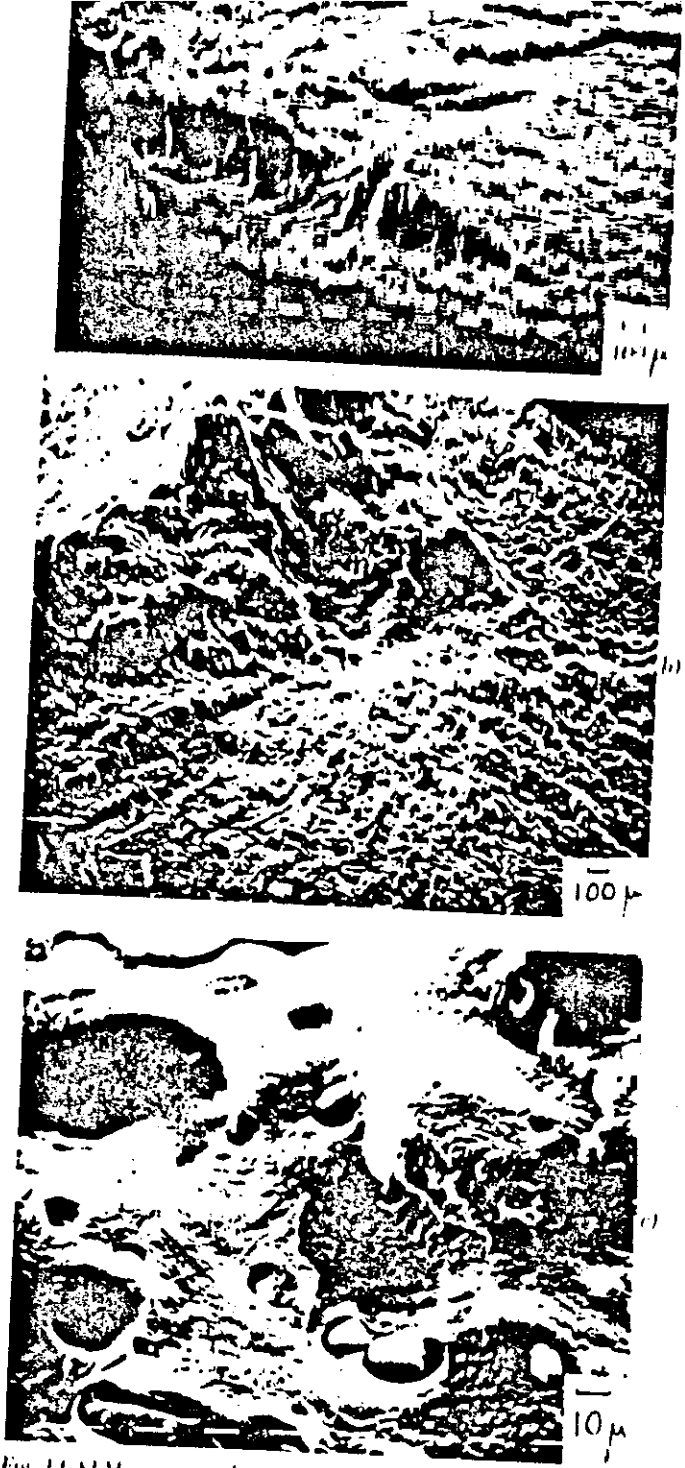

Fig. 14. SEM micrographs of Bs fracture surfaces at different test temperatures
a) −20 °C (40×)
b) +3.5 °C (40×)
c) +3.5 °C initiation region (640×)

R. This is certainly due to the total rubber content (10 percent in weight), which is insufficient to reinforce suitably the PA6 at those temperatures. Such behavior is in agreement with the fractographic analysis that shows fracture mode characterized by a fast crack propagation involving the whole sample (see *Figs. 9a, 10a,* and *11a*).

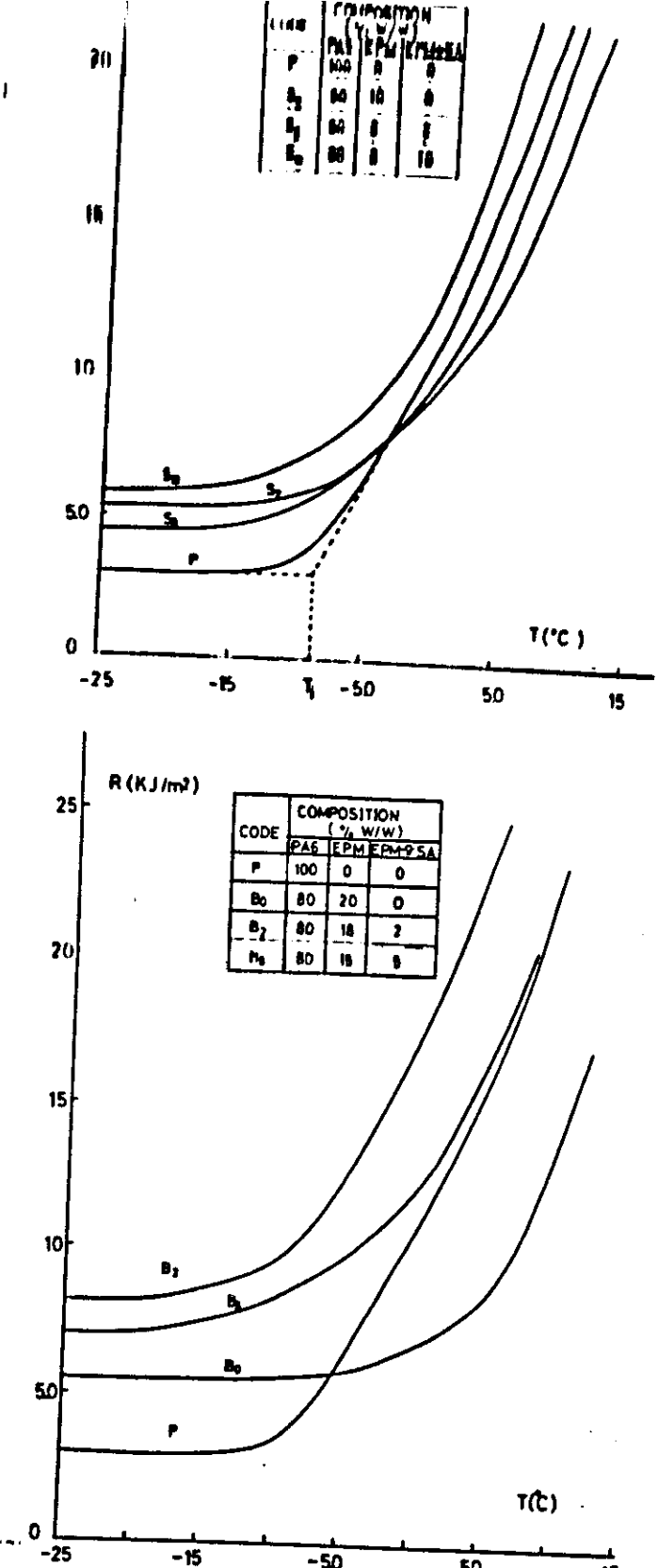

Fig. 15. Impact resistance (R) for PA6, binary and ternary blends at different testing temperatures. a) "S" samples; b) "B" samples.

Moreover, for *S* blends the brittle-ductile transition temperature seems to be scarcely dependent on the rubber content as well as on the nature of the added rubber. For all the range of temperatures

that of transition, such blends show a larger ductile flow region with respect to the other two systems (see *Figs. 9c, 10c,* and *11c*) where it is possible to dissipate a large amount of fracture energy by plastic deformation.

The impact properties of the B_0 blend are characterized, at lower temperatures, by R values only slightly higher than those of the S_0 blend and pure PA6 and by a brittle-ductile transition shifted towards a temperature that is higher than that of any other investigated blend. Such behavior may be related to the large dimensions of the rubbery dispersed domains and to the very poor adhesion with the PA6 matrix.

As shown by *Fig. 15b*, the B_2 and B_5 coded blends show, at temperatures below the transition, R values about 3 and 2 times higher than that of pure PA6, respectively. At higher temperatures beyond the transition, the R value of B_2 is also larger than that of B_5.

It is somewhat surprising that the B_2 blend, containing only 2 percent of the functionalized rubber, shows better impact properties than the B_5 blend. The finding that the B_2 blend, containing only 2 percent modified EPM g SA rubber, exhibits better impact properties than any other blend investigated cannot be accounted for by a particularly high degree of adhesion between matrix and dispersed domains, as the latter are completely removed by boiling xylene (see *Fig. 6*). Such behavior is more likely to be related to an optimum size distribution of dispersed domains produced together with a rather drastic modification of intrinsic matrix properties following a process of "dissolution" of (EPM-g-SA)-g-PA6 copolymer and/or nucleation effects that gives rise to PA6 spherulites with lower dimensions and different structure of the interspherulitic boundary regions (3). Optical observations of thin sections of PA6 and B_2 blends show that in the case of the blend sample the dimensions of the PA6 spherulites are indeed smaller than those observed in plain PA6.

For the sake of comparison, in *Fig. 16*, the impact behavior of B_2 and B_5 blends is compared with that of a ternary PA6/EPM/EPM-g-SA 80/15/5 blend prepared by melt-mixing of components (3). From the examination of the trend of the curves in *Fig. 16*, it emerges that the impact properties of B_2 and B_5 are slightly better than those of blends obtained by melt-mixing. This finding is in agreement with the SEM observations that indicate a rather similar overall morphology of the samples (3).

CONCLUDING REMARKS

Caprolactam polymerization via anhydrolytic process may be carried out in the presence of rubbery components such as EPM and/or modified

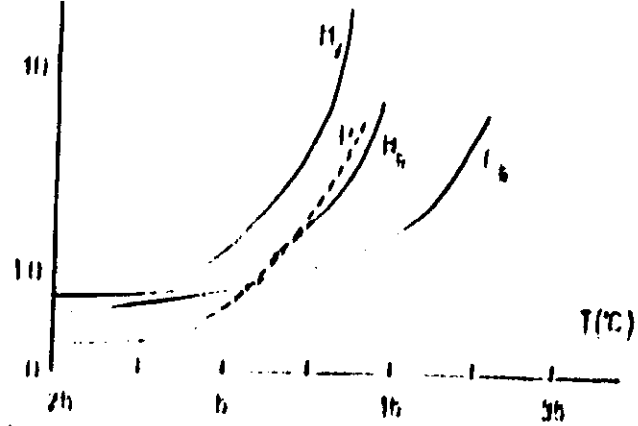

Fig. 16. Comparison of impact behavior of PA6 and B_2, B_5 blends with a PA6/EPM/EPM g SA (80/15/5) ternary blend prepared by melt mixing process (Curve C_3). Blend C_3 was obtained by melt mixing the components in Brabender-like apparatus at 260°C with a mixing time of 20 min and rotational speed rollers of 32 rpm

EPM(EPM g SA). Two different methods of blends preparation were followed: the first (solution method, "S" coded blends) involved a preliminary dispersion of the rubber in a suitable solvent able to dissolve the caprolactam and the initiator. The second (bulk method, "B" coded blends) is characterized by the fact that the rubber is directly added to caprolactam and initiator and dispersed by mechanical stirring before polymerization. It is found that the degree of conversion of caprolactam to PA6 and molecular mass are practically independent of the content of functionalized EPM-g-SA.

Tensile strengths and elongations at break of binary and ternary blends are slightly lower than those of pure PA6. A more marked positive effect on the impact properties of PA6 is found when a small amount of EPM-g-SA (2 and 5 percent) is added to binary PA6/EPM (80/18) or (80/15) blends. Better impact behavior was obtained in the case of the B_2 blend (PA6/EPM/EPM-g-SA 80/18/2).

Evidence mainly supported by morphological and structural analysis shows that EPM-g-SA acts as an emulsifier and interfacial stabilizer between the matrix PA6 and the dispersed main component EPM. As a matter of fact, a more fine dispersion of the rubbery component is observed in blends containing a certain amount of functionalized EPM-g-SA rubber.

The interfacial activity of EPM-g-SA is due to a true chemical reaction with growing PA6 chains through the formation of a graft copolymer of the (EPM-g-SA)-g-PA6 type.

Finally it must be pointed out that the main advantage of the method of blend preparation described in the present paper resides on the fact that with a suitable reactor the number of overall operations is reduced with respect to the melt-mixing preparation. Nevertheless, the properties of the blends obtained are similar. We wish to emphasize

that with better control of the reaction variables, it should be possible to produce blends with different modes and states of dispersion of the rubbery components simply by changing the reaction conditions, stirring power, and starting composition.

ACKNOWLEDGMENT

This work was partly supported by the Finalyzed Project on Fine Chemistry of the Italian C.N.R.

REFERENCES

1. L. Amelino, S. Cimmino, R. Greco, N. Lanzetta, G. Maglio, M. Malinconico, E. Martuscelli, R. Palumbo, and C. Silvestre, Preprints of "Plasticon 81-Polymer Blends", p. 14.1, Warwick, 1981.
2. S. Cimmino, L. D'Orazio, R. Greco, G. Maglio, M. Malinconico, E. Martuscelli, C. Mancarella, R. Palumbo and G. Ragosta, *Polym. Eng. Sci.*, in press.
3. A. Casale, F. Sperroni, A. Filippi, E. Martuscelli, R. Greco, R. Palumbo, G. Maglio, M. Malinconico, N. Lanzetta, G. Ragosta, L. D'Orazio, Patent N°. 21204A/84.
4. M. I. Kohan, "Macromolecular Syntheses", J. A. Moore Ed., *Collective Vol. 1*, p. 93, John Wiley & Sons, N.Y., (1977).
5. J. Sebenda, *J. Macromol. Sci. Chem., A6*, 1145, (1972).
6. G. Illing, "Polymer Blends, Processing, Morphology and Properties", E. Martuscelli, R. Palumbo and M. Kryszewski, Eds., p. 167, Plenum Press, N.Y., (1980).